PHYSICAL REVIEW A VOLUME 8, NUMBER 3 SEPTEMBER 1973

Precision Experiments on Muonium. III. Ramsey Resonance in Zero Field

D. Favart,* P. M. McIntyre,† D. Y. Stowell,‡ V. L. Telegdi, and R. DeVoe§
The Enrico Fermi Institute and Department of Physics, The University of Chicago, Chicago, Illinois 60637

R. A. Swanson
Department of Physics, University of California, San Diego, La Jolla, California 92037

(Received 29 March 1973)

A novel method for measuring the hyperfine interval $\Delta\nu$ of muonium in zero magnetic field is described. It consists in applying two successive coherent microwave pulses (lengths τ, separation $T+\tau$) to muonium, and observing the change in muon polarization at $t>T+2\tau$. By linearly extrapolating two low-pressure runs in Kr together with earlier Chicago data, we obtain $\Delta\nu(0)=4463\,301.2(2.3)$ kHz (0.5 ppm). A joint fit of all available data in Ar and Kr yields $\Delta\nu(0)=4463\,304.4(2.3)$ kHz. With $\mu_\mu/\mu_p=3.183\,349(15)$ the latter implies (a) $\alpha^{-1}-137=0.036\,31(32)(2.4\text{ ppm})$, and (b) a proton polarizability $\delta_p'=5.4(4.8)$ ppm.

I. INTRODUCTION

This experiment is the third of a series[1,2] of resonance experiments on muonium at the University of Chicago. The primary goal of the series is a consistent measurement of the ground-state hyperfine structure interval $\Delta\nu$ and the muon magnetic moment $\mu_\mu=\frac{1}{2}g_\mu'\mu_B$. These two quantities allow a very precise determination of the fine-structure constant α; alternatively, using the current value of α from other sources they provide a stringent test of quantum-electrodynamical (QED) corrections to the Fermi formula for $\Delta\nu$.

The present experiment had two particular purposes: (i) to develop a novel, statistically powerful resonance technique for measuring $\Delta\nu$; (ii) to measure $\Delta\nu$ at the lowest practical gas densities, in order to minimize the importance of extrapolation procedures used for eliminating the effects of the buffer gas on $\Delta\nu$.

The principle used here to detect muonium transitions is the same as in all precision muonium experiments: A polarized muon (μ^+) stops in a noble gas, where it captures an electron to form muonium in the ground state with the muon polarization partially preserved. An applied microwave field at or near resonance causes a transition involving a spin-flip of the muon. This transition is detected by measuring the change in the positron decay asymmetry which accompanies the spin-flip.

$\Delta\nu$ can be obtained by several resonance techniques. We will briefly describe each alternative, and discuss its merits in terms of the error in $\Delta\nu$ for a given number of muon decays. The first Chicago experiment[1] studied the Zeeman transition $(F, M_F)=(1,1)\rightarrow(1,0)$ at the "magic field" $B_0=11\,327$ G where first-order field dependence of the transition frequency $\nu_1\simeq 1923$ MHz vanishes. This resonance does not provide a measurement of g_μ', so that an independent value of g_μ' must be used to obtain $\Delta\nu$ and α (the effect of an error in g_μ' is, however, reduced a factor 14 in $\Delta\nu$ at the magic field). The statistically optimum linewidth using this method is 300 kHz. We term the error on $\Delta\nu$ using this method σ_L.

In the double-resonance experiment,[2] the transitions $(1,1)\rightarrow(1,0)[\nu_1]$ and $(1,1)\rightarrow(0,0)[\nu_2]$ were induced simultaneously, and resonance was observed in the sum ν_+ and difference ν_- of ν_1, ν_2. The signal and linewidth are both doubled relative to those for a single transition (the statistically optimum linewidth is 500 kHz). The sum frequency ν_+ gives $\Delta\nu$ directly ($\nu_+\equiv\Delta\nu$), with an error $\sigma_{DR}=\sigma_L$. The $\Delta\nu$ thus obtained does not require knowledge of g_μ'; in fact, the ν_- resonance together with ν_+ gives a precise independent measurement of g_μ'.

The Yale group has measured $\Delta\nu$ directly by inducing the transitions $(1,\pm1)\rightarrow(0,0)$ in zero external field.[3,4] The $(1,\pm1)$ states are degenerate, so that the transitions are induced concurrently. In the ideal case, the linewidth for optimum statistical power would be 280 kHz, 60% of that in double resonance, while the signal would be 40% of the double-resonance signal, so that $\sigma_{ZF}=1.5\sigma_L$. In practice, stability problems required the use of twice the optimum linewidth,[4] resulting in a statistical power about half that of the double-resonance method. No measurement of the muon moment is possible in zero field, so an independent value of this quantity must be used to obtain α.

In this paper we describe a zero-field resonance technique which produces a linewidth narrower

than that in any of the methods described above (in fact, narrower than the "natural" linewidth $\gamma/2\pi$ = 140 kHz). The statistical power of this technique is at least ten times that of an optimized conventional resonance in zero field. The latter bears roughly the same relation to the novel method as the Rabi resonance (single oscillating field) for atomic beams does to its modification by Ramsey (two separated oscillating fields).[5,6] In fact, this work was strongly inspired by that of Ramsey and his associates.

We shall now examine the novel technique qualitatively making reference to Fig. 1. Assume that muons with initial polarization $P_z(0)=1$ form muonium in the (1, 1) state in zero field. A microwave field $\vec{B}_1$ oscillating in the $\hat{x}$ direction with circular frequency $\omega \simeq \omega_0 = 2\pi\Delta\nu$ will induce transitions to the (0, 0) ground state, and from it back to both $|M_F|=1$ states. $P_z(t)$ will reach -1 when only the (1, -1) state is populated, and $+1$ when only the (1, 1) state is populated. $P_z(\tau)=0$ at a time τ when the (1, ±1) states are equally populated. If $\vec{B}_1$ is switched off at τ, $\vec{P}$ will oscillate along $\hat{y}$ with frequency ω_0 because we have prepared a coherent superposition of $F=1$ and $F=0$ states. $\vec{B}_1$ is switched on again after a time T. $\vec{P}$ then rotates to $P_z=-1$ after a time τ only if $\vec{B}_1$ and $\vec{P}$ are in the same phase relation at $t=T+\tau$ as they were at $t=0$. If the two microwave pulses are coherent, this implies an interference condition for $\Delta=\omega_0-\omega$. It has the form

$$P_z(\Delta) = -\cos\Delta(T+\tau), \tag{1}$$

with a "linewidth" $\Gamma=\pi/(T+\tau)$. For the pulse separation $T+\tau=3.4$ μsec used in the present experiment, $\Gamma/2\pi=150$ kHz.

The improvement in linewidth makes the split-field technique a very powerful one for precision measurement of $\Delta\nu$.[7] Furthermore, as discussed in Sec. IV, we have been unable to locate any source of systematic error, of either physical or instrumental origin, at a level of ≤ 0.2 ppm.

Previous experiments[4,8] have investigated the effects of the buffer gas on the measured $\Delta\nu$ in terms of linear and quadratic pressure shifts. In order to further test the validity of the extrapolation to zero density, we performed the present experiment in two different noble gases, and extrapolated them independently.

II. PRINCIPLE OF EXPERIMENT

The primary object of our experiment is to measure $\Delta\nu$. $\Delta\nu$ is given by[9]

$$\Delta\nu = \left(\tfrac{4}{3}\alpha^2 \mathcal{R}_\infty c g_s g'_\mu\right)\left(1+m_e/m_\mu\right)^{-3}\left(1+\epsilon_{\rm QED}\right). \tag{2}$$

The first two parentheses are the nonrelativistic Fermi formula, the second being the reduced mass correction, and

$$g_s = 2\mu_e/\mu_B,\quad g'_\mu = g_\mu(m_e/m_\mu) = 2\mu_\mu/\mu_B. \tag{3}$$

The third parentheses contain all higher-order corrections:

$$\epsilon_{\rm QED} = \tfrac{3}{2}\alpha^2 + \epsilon_1 + \epsilon_2 + \epsilon_3 + \delta_{\mu 1} + \delta_{\mu 2}. \tag{4}$$

All terms except $\frac{3}{2}\alpha^2$ are QED corrections: ϵ_1, ϵ_2, ϵ_3 are higher-order radiative terms and $\delta_{\mu 1}$, $\delta_{\mu 2}$ (Ref. 10) are due to relativistic recoil effects. $\frac{3}{2}\alpha^2 = 79.88$ ppm is the relativistic (not QED) correction to the Schrödinger equation;

$$\begin{aligned}
&\epsilon_1 = \alpha^2\left(\ln 2 - \tfrac{5}{2}\right) = -96.22 \text{ ppm},\\
&\epsilon_2 = -(8\alpha^3/3\pi)\ln\alpha\left(\ln\alpha + \frac{281}{480} - \ln 4\right) = -9.29 \text{ ppm},\\
&\epsilon_3 = 18.4\alpha^3/\pi = 2.28 \text{ ppm},\\
&\delta_{\mu 1} = (3\alpha/\pi)(m_e/m_\mu)\left[1-(m_e/m_\mu)^2\right]^{-1}\\
&\qquad \times \ln(m_e/m_\mu) = -179.7 \text{ ppm},\\
&\delta_{\mu 2} = \tfrac{9}{2}\alpha^2(m_e/m_\mu)(1+m_e/m_\mu)^{-2}\ln\alpha^{-1} = 5.6 \text{ ppm}.
\end{aligned} \tag{5}$$

Using the recommended values[11,12] of the fundamental constants and $m_\mu/m_e = 206.76670(93)$ from our double-resonance experiment,[2] we have

$$\Delta\nu = \alpha^2\mu_\mu/\mu_p[26.329557(10)\times 10^9] \text{ kHz}. \tag{6}$$

With the current value of $\alpha_{\rm WQED}$[11] and the value of μ_μ/μ_p reported by Hague *et al.*,[13] one obtains $\Delta\nu$ = 4463 316(16) kHz.

A. Split Field Resonance with Square Pulses

Consider a muonium atom which at $t=0$ is subjected to a microwave field $\vec{B}_1 = B_1\hat{x}\cos\omega t$ (the muon polarization axis is again $\hat{z}$). The interaction Hamiltonian in this field is

$$H' = \tfrac{1}{2}\mu_B(-g_s\vec{J} + g'_\mu\vec{S}_\mu)\cdot\vec{B}_1, \tag{7}$$

where $\vec{J}$ and $\vec{S}_\mu$ are the electron and muon spin operators. The (F, M_F) states are eigenstates of this Hamiltonian in zero static field:

$$\begin{aligned}
&(1,1) = \alpha_\mu\alpha_e, \quad (1,0) = (\alpha_\mu\beta_e + \beta_\mu\alpha_e)/\sqrt{2},\\
&(1,-1) = \beta_\mu\beta_e, \quad (0,0) = (\alpha_\mu\beta_e - \beta_\mu\alpha_e)/\sqrt{2}.
\end{aligned} \tag{8}$$

When a muon of polarization P_μ captures an unpolarized electron to form muonium, the (F, M_F) states are populated as follows:

$$P_{11}=\tfrac{1}{4}(1+P_\mu),\quad P_{10}=\tfrac{1}{4},\quad P_{1-1}=\tfrac{1}{4}(1-P_\mu),\quad P_{00}=\tfrac{1}{4}. \tag{9}$$

The resulting polarization of the muon in muonium is thus $P_z(0)=\frac{1}{2}P_\mu$.

The (F, M_F) states are represented by their amplitudes $a_{FM_F}(t)$, and have energy levels $E_{F=1}=\hbar\omega_0$, $E_{F=0}=0$. The driving field can be decomposed into its circular components: $\vec{B}_1=\frac{1}{2}B_1\hat{x}(e^{i\omega t}+e^{-i\omega t})$; with $\omega\simeq\omega_0$, the second term is resonant, while the first is counterresonant (Bloch-Siegert effect)[14] and may be discarded. The time-dependent Schrödinger equations are

$$\begin{aligned} i\dot{a}_{11}&=(\omega_0-\tfrac{1}{2}i\gamma)a_{11}+\Omega e^{-i\omega t}a_{00},\\ i\dot{a}_{10}&=(\omega_0-\tfrac{1}{2}i\gamma)a_{10},\\ i\dot{a}_{1-1}&=(\omega_0-\tfrac{1}{2}i\gamma)a_{1-1}-\Omega e^{-i\omega t}a_{00},\\ i\dot{a}_{00}&=(-\tfrac{1}{2}i\gamma)a_{00}+\Omega e^{i\omega t}(a_{11}-a_{1-1}), \end{aligned} \tag{10}$$

$$\hbar\Omega=(g_s-g'_\mu)\mu_B B_1/4\sqrt{2}, \tag{11}$$

where the terms in $\gamma=1/\tau_\mu$ represent the decay of the muon. It is convenient to work in the interaction representation, defining new amplitudes A_i:

$$\begin{aligned} A_+&=e^{i(\omega_0-i\gamma/2)t}(a_{11}+a_{1-1})/\sqrt{2},\\ A_-&=e^{i(\omega_0-i\gamma/2)t}(a_{11}-a_{1-1})/\sqrt{2},\\ A_{10}&=e^{i(\omega_0-i\gamma/2)t}a_{10},\\ A_{00}&=e^{\gamma t/2}a_{00}. \end{aligned} \tag{12}$$

The equations of motion for A_i are

$$\begin{aligned} i\dot{A}_+&=0,\quad i\dot{A}_-=be^{i\Delta t}A_{00},\\ i\dot{A}_{10}&=0,\quad i\dot{A}_{00}=be^{-i\Delta t}A_-, \end{aligned} \tag{13}$$

where $b\equiv\sqrt{2}\Omega$ and $\Delta\equiv\omega_0-\omega$. In convenient units, $b/2\pi(\mathrm{MHz})=0.8\,B_1(\mathrm{G})$. The amplitudes A_+, A_{10} are constants of motion, while A_-, A_{00} satisfy the classic Rabi equations. The quasi-two-level nature of the system results from the degeneracy of the $F=1$ states.

The solutions of Eq. (13) at a time $t+t_0$, in terms of the amplitudes at time t_0, are

$$\begin{aligned} \sqrt{2}\,A_-(t+t_0)&=e^{i\Delta t/2}[F(t)A_-(t_0)+e^{i\Delta t_0}G(t)A_{00}(t_0)],\\ \sqrt{2}\,A_{00}(t+t_0)&=e^{-i\Delta t/2}[e^{-i\Delta t_0}G(t)A_-(t_0)+F^*(t)A_{00}(t_0)],\\ F(t)&=\cos\tfrac{1}{2}at-i(\Delta/a)\sin\tfrac{1}{2}at,\\ G(t)&=-i(2b/a)\sin\tfrac{1}{2}at,\\ a&=+(\Delta^2+(2b)^2)^{1/2}. \end{aligned} \tag{14}$$

Note that the factors $e^{\pm i\Delta t_0}$ account for the phase of the microwave field at t_0. We will consider the case of an initially fully polarized muon:

$$A_-(0)=A_+(0)=1/\sqrt{2},$$

$$A_{10}(0)=A_{00}(0)=0,\quad P_z(0)=1.$$

Since in the experiment one detects a polarization change $\Delta P_z=P_z(0)-P_z(t)$, the quantity of interest is

$$\begin{aligned} P_z(t)&=(|a_{11}|^2-|a_{1-1}|^2)/\textstyle\sum|a_i|^2=e^{\gamma t}(a_{11}a_{11}^*-a_{1-1}a_{1-1}^*)\\ &=A_-A_+^*+A_-^*A_+=2A_+(0)\,\mathrm{Re}A_-(t)=\sqrt{2}\,\mathrm{Re}A_-. \end{aligned} \tag{15}$$

We now iterate Eq. (14) for the case of two coherent square pulses of length τ and separation $T+\tau$. After the first pulse, with initial rf phase zero,

$$\begin{aligned} \sqrt{2}\,A_-(\tau)&=e^{i\Delta t/2}F(\tau),\\ \sqrt{2}\,A_{00}(\tau)&=e^{-i\Delta t/2}G(t),\\ P_z(\tau)&=\mathrm{Re}[e^{i\Delta t/2}F(\tau)]. \end{aligned} \tag{16}$$

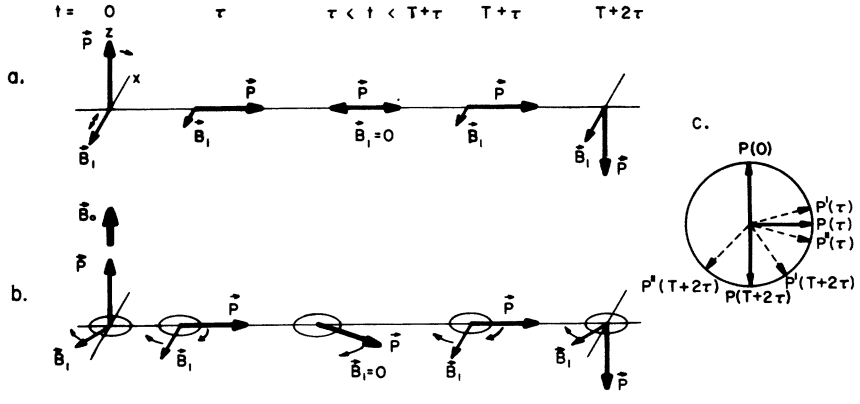

FIG. 1. Motion of the polarization P in the split-field resonance. (a) Ramsey 2-level split-field resonance; (b) the 3-level resonance of the present experiment; and (c) effect on final polarization of rf field inhomogeneities. P shows the evolution of the polarization for $\frac{1}{2}\pi$ pulses; P' at a point where B_1 is weaker, P'' at a point where B_1 is stronger.

As explained in the Introduction, we wish to choose the width τ and field b so that $P_z(\tau)=0$. The condition $a\tau=\pi$, together with the requirement $b\gg\Delta$, yields $F(\tau)=0$, $P_z(\tau)=0$. We will term such pulses "$\frac{1}{2}\pi$ pulses," since they bring the polarization into the transverse plane.

A_- and A_{00} are constant during the rf off period; this is a convenient artifact of the interaction representation.

The two rf pulses are coherent, being excited from a single free-running oscillator. We introduce an additional phase shift φ into the second pulse, so that its phase at $t=T+\tau$ becomes $\omega(T+\tau)+\varphi$. The amplitudes A_-, A_{00} at the end of the second pulse are then given by

$$\sqrt{2}\,A_-(T+2\tau)=e^{i\Delta\tau}F^2(\tau)+e^{i\Delta(T+\tau)+i\varphi}G^2(\tau), \tag{17}$$

$$\sqrt{2}\,A_{00}(T+2\tau)=e^{-i\Delta(T+\tau)-i\varphi}F(\tau)G(\tau)+e^{-i\Delta\tau}F^*(\tau)G(\tau)$$

and the corresponding polarization is

$$P_z(T+2\tau)=\mathrm{Re}[e^{i\Delta\tau}F^2(\tau)+e^{i\Delta(T+\tau)+i\varphi}G^2(\tau)]. \tag{18}$$

For $\frac{1}{2}\pi$ pulses,

$$F(\tau)=-i\Delta/a,\quad G(\tau)=-i(2b/a);$$

$$P_z(T+2\tau)=-(\Delta/a)^2\cos\Delta\tau - (2b/a)^2\cos[\Delta(T+\tau)+\varphi]. \tag{19}$$

In the limit $b\gg\Delta$ and with $\varphi=0$, we recover Eq. (1).

The polarization change ΔP_z is detected via the well-known backward-forward asymmetry of the decay positrons. The distribution of decay positrons at an angle θ to the muon polarization axis is

$$N(\theta)=N_0[1+AP_z(T+\tau)\cos\theta], \tag{20}$$

where A is the momentum-averaged decay asymmetry ($A=\frac{1}{3}$), and serves as a detector for changes in P_z.

We form a signal from two equal samples of data with rf phase shift $\phi=\pm\frac{1}{2}\pi$, which is the most useful case in practice[15]:

$$S_2(\Delta)=(N_+-N_-)/(N_++N_-)=AP_z(0)(2b/a)^2\times\cos\theta\sin\Delta(T+\tau). \tag{21}$$

The peak signal is $S_0=AP_z(0)\langle\cos\theta\rangle$, with $\cos\theta$ averaged over the acceptance of the decay positron telescope. $S_2(\Delta)$ is a sinusoid modulated by a Lorentzian envelope $(2b/a)^2$. It has three distinctive features: (i) it crosses zero at resonance ($\Delta=0$) and hence has maximum slope there; (ii) it has a FWHM $\Gamma/2\pi=50$ kHz for the pulse separation $T+\tau=3.4$ μsec; (iii) both samples of data are taken with rf *on*, and thus contribute directly to the determination of $\Delta\nu$. In a conventional resonance, half the data are taken with rf *off* for normalization.

To choose the rf pulse amplitude b and length τ so that $a\tau=\pi$, we first perform a single-pulse experiment. Equation (16) with the requirement $b\gg\Delta$, yields

$$P_z(\tau)=\cos\tfrac{1}{2}\Delta\tau\cos b\tau. \tag{22}$$

We set $\Delta=0$, and vary either b or τ, keeping the other one constant. The signal observed in the conventional rf on/off fashion is

$$S_1(b\tau)=(N_{\mathrm{on}}-N_{\mathrm{off}})/N_{\mathrm{on}}+N_{\mathrm{off}})=S_0\sin^2\tfrac{1}{2}b\tau. \tag{23}$$

The condition $b\tau=\frac{1}{2}\pi$ defines the half-height value of $S_1(b\tau)$, thus providing an empirical means for meeting the $\frac{1}{2}\pi$ pulse requirement.

B. Statistical Considerations

We wish to compare the present technique with its precursors[1-4] in terms of statistical power. In Appendix A, we optimize the experimental parameters for each technique to give minimum error on $\Delta\nu$. The error resulting in each case is discussed below for a sample of N_e observed decays.

a. *Conventional 2-level cw resonance.* If one uses a cw microwave field to excite one of the Zeeman transitions (ν_i),[1] the signal formed is

$$S_L(\Delta)=S_0(2b)^2/2(a^2+\gamma^2). \tag{24}$$

If one optimizes b and the range of Δ, the error σ_L in the determination of $\Delta\nu$, in terms of the total number N_e of decay positrons detected, is

$$\sigma_L(\Delta\nu)=1.56/S_0\tau_\mu\sqrt{N_e}. \tag{25}$$

b. *Double resonance.* In method a, half of the muons are unaffected by the rf field, because they populate a nonresonant level. By exciting both transitions simultaneously,[2] both signal and linewidth double. The error on $\Delta\nu$ is hence

$$\sigma_{\mathrm{DR}}(\Delta\nu)=\sigma_L(\Delta\nu). \tag{26}$$

This technique also allows measurement of g'_μ, which makes it quite attractive for future work.[7]

c. *Zero-field* cw *resonance.* The signal in a conventional rf on/off resonance in zero field[3,4] is obtained by integrating $P_z(t)$ of Eq. (16):

$$S_{ZF}(\Delta)=\tfrac{1}{2}S_0\int_0^\infty e^{-\gamma t}\,\mathrm{Re}[e^{i\Delta t/2}F(t)-1]\,\gamma dt=\tfrac{1}{2}S_0(2\gamma)^2[(2\gamma)^2+(a+\Delta)(a-\Delta)]/[(2\gamma)^2+(a+\Delta)^2][(2\gamma)^2+(a-\Delta)^2]. \tag{27}$$

An important feature of Eq. (27) is that $S(\Delta)$ is *not* a Lorentzian, and that its width is proportional to the rf *power*, while the width of a Lorentzian is proportional to the rf *field*. The Yale group has evaluated Eq. (27) in terms of the peak signal and FWHM as a function of rf power; Figs. 27 and 28 of Ref. 3(b) show the results. Using those data, we find the optimum error in $\Delta\nu$ is

$$\sigma_{ZF}(\Delta\nu) = 1.50\,\sigma_L(\Delta\nu) = 2.32/S_0\tau_\mu\sqrt{N_e}\ . \tag{28}$$

At the optimized rf power, the peak signal is about half its saturated value; this is a property of the non-Lorentzian line shape noted above. In practice, stability problems require the use of twice the optimum power, making $\sigma_{ZF} \simeq 2\sigma_L$.

d. Split-field resonance in zero field. A dramatic increase in statistical power is achieved by using our split-field technique, owing to the following facts: (i) The signal height doubles because the polarization goes from +1 to −1 instead of from +1 to 0; (ii) the linewidth Γ_{SF} is far narrower than in any conventional resonance; (iii) by taking data with phase shifts $\varphi = \pm\frac{1}{2}\pi$, instead of rf on and rf off, one gains a second doubling of the effective signal height; (iv) the linewidth is power independent, so one can saturate the signal, whereas in conventional resonance one limits rf power to avoid excessive linewidth.

On the other hand, one gets no signal from positrons decaying before the end of the second rf pulse; this limits T to 2τ or less. By optimizing the parameters, one obtains

$$\sigma_{SF}(\Delta\nu) = 0.22/S_0\tau_\mu\sqrt{N_e}. \tag{29}$$

The split-field resonance is more sensitive than other techniques to the variation of rf field over the volume of the cavity, as will be discussed in Sec. II E. The *effective* peak signal under our experimental conditions is 51% of its ideal value:

$$\sigma_{SF}(\Delta\nu) = 0.42/S_0\tau_\mu\sqrt{N_e}. \tag{30}$$

One can now compare the statistical powers ($\sim 1/\sigma^2$) of the four optimized resonance techniques; first, for each method idealized,

$$\text{L}:\text{DR}:\text{ZF}:\text{SF} = 1:1:0.45:50\,, \tag{31}$$

and second, for each method as actually performed,

$$\text{L}:\text{DR}:\text{ZF}:\text{SF} = 1:1:0.25:12.5\,. \tag{32}$$

C. Description of the Experiment

The π^+ beam in the muon channel of the University of Chicago synchrocyclotron produced a "backward decay" μ^+ beam with $p_\mu = 75$ MeV/c, and a measured polarization $P_\mu = 55\%$. We selected this beam with a wedge bending magnet, collimated it to 12 cm diam, and stopped it in a pressure vessel (see Fig. 2). The vessel contained the microwave cavity in a noble-gas environment, either Ar or Kr, and was carefully shielded to produce "zero" static magnetic field over the volume of the cavity.

The stopped muon captures an electron to form muonium in the ground state. No subsequent depolarization can occur by spin-exchange with the electrons of gas atoms, since in a noble gas all electrons are paired.

A scintillation-counter telescope, in conjunction with two proportional counters located within the pressure vessel, defined a stopping muon and its decay positron. The muon stop signature triggered the double-pulse microwave pattern, with $\varphi = \pm\frac{1}{2}\pi$ relative phase shift on alternate cyclotron beam pulses. It also initiated a timing sequence which was terminated by the decay positron signature (this was actually done in inverted order, as explained in Sec. III). The decay time was recorded together with an identification of the decay according to four categories: $\varphi = \pm\frac{1}{2}\pi$ forward decay, and $\varphi = \pm\frac{1}{2}\pi$ backward decay. In effect, one performs two separate resonance experiments simultaneously—one in each decay hemisphere. Only the decays which occur after the second rf pulse ($t > T + 2\tau$) were used in forming the signal $S_2(\Delta)$.

D. Calculation of Expected Signal

We wish to calculate the magnitude of the peak signal for the split-field resonance. $P_z(T+2\tau)$ of Eq. (18) produces a signal

$$S_2'(\Delta) = A P_z(0)(2b/a)^2 \langle \cos\theta \rangle \sin^2 b\tau \sin\Delta(T+\tau)\,. \tag{33}$$

The rf field b resonates in the TM_{050} mode of the cavity, with a cylindrically symmetric spatial distribution

$$b(r) = b_0 J_1(15r/R)\,, \tag{34}$$

where R is the cavity radius. We must average S_2' over the cavity volume, weighting with the normalized distribution ρ_e of decay positrons detected by the counter telescope from a given decay point P. If $\langle\Omega\rangle$ is the acceptance solid angle at P of the counter telescope and ρ_μ is the distribution of stopping muons, then

$$\rho_e = (\langle\Omega\rangle\rho_\mu)_{\text{detector average}}\,. \tag{35}$$

ρ_μ was measured in a previous experiment ($B = 0$ case in Fig. 10 of Ref. 1) for the same beam and location as used in the present experiment. $\langle\Omega\rangle$ and $\langle\cos\theta\rangle$ were calculated for the geometry of the cavity and counter telescope. Figure 3 shows the resulting ρ_e. The final expression for the peak signal is

$$\langle S_0\rangle = AP_z(0)[\rho_e(2b/a)^2\langle\cos\theta\rangle \sin^2 b\tau]_{\text{cavity average}}. \tag{36}$$

We choose the rf pulse width τ from the results of a single-pulse experiment, with signal given by Eq. (23) and averaged over the cavity:

$$\langle S_1(b_0\tau)\rangle = -AP_z(0)[\rho_e\langle\cos\theta\rangle \sin^2\tfrac{1}{2}b\tau]_{\text{cavity average}}. \tag{37}$$

$\langle S_1(b_0\tau)\rangle$ was calculated numerically,[16] and is plotted in Fig. 14 together with the data from the single-pulse resonance in 6469 Torr of Kr. The field b_0 corresponds to the maximum output power of the TWT (see Sec. III A) $b_0/2\pi = 7.4$ MHz. The peak of $\langle S_1\rangle$ corresponds to an averaging of the condition $b\tau = \pi$ over the cavity, and occurs at $\tau = 0.38$ μsec. The averaged $\frac{1}{2}\pi$ pulse condition occurs at $\tau = 0.23$ μsec; we used this pulse length in the actual experiment.

The signal $\langle S_0\rangle$ is diluted by muons stopping in the lateral walls (aluminum) of the cavity, rather than in the gas. The detection system accepts them as legitimate events. It also accepts a fraction of the muons stopping in the downstream pressure vessel window (also aluminum), because

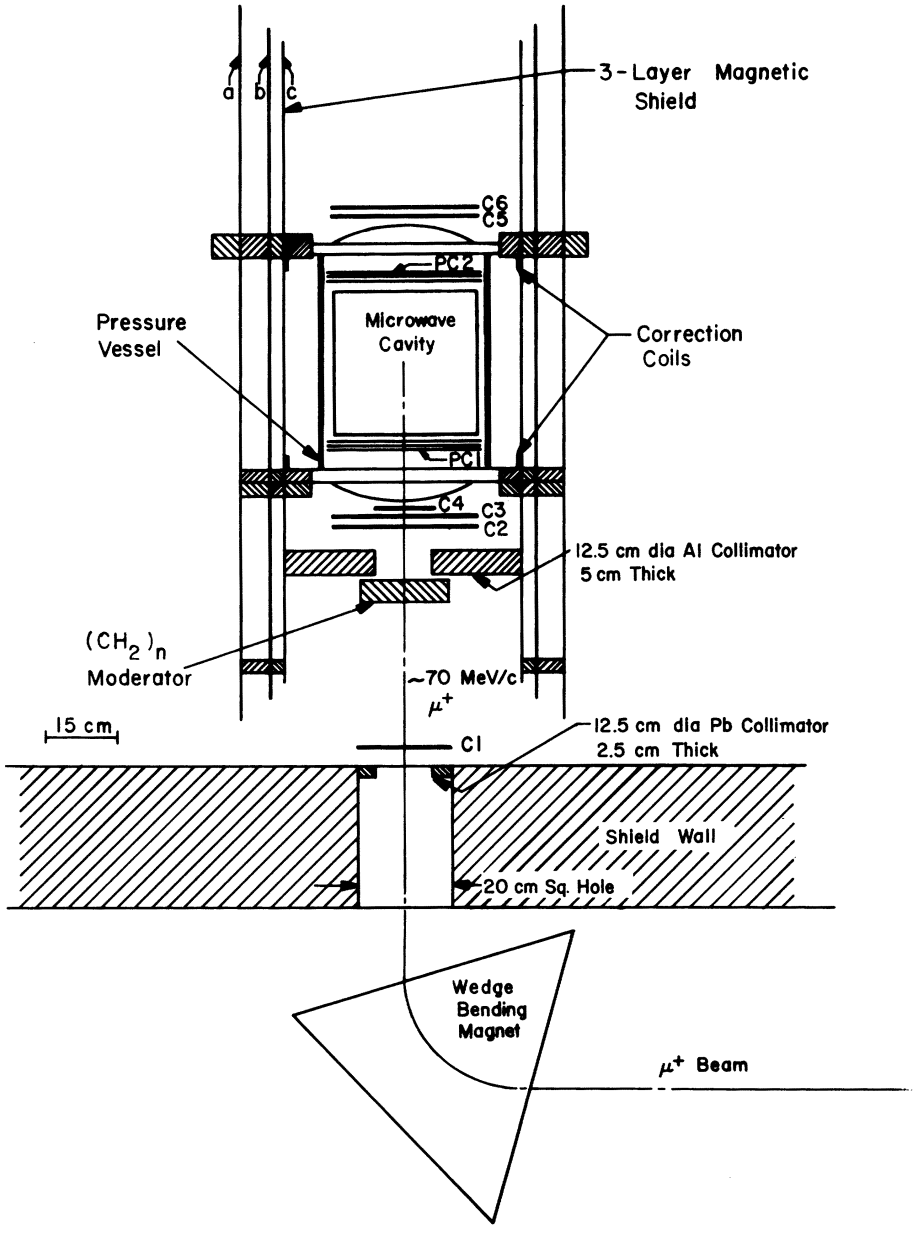

FIG. 2. Experimental arrangement. The magnetic shielding layers *a*, *b*, *c* have thicknesses 0.12 cm, 0.16 cm, 0.35 cm, respectively.

of inefficiency of the downstream veto proportional counter. The decays from these two classes of stopping muons carry no signal, and dilute the observed signal by the ratio $f=N_{\rm gas}/(N_{\rm gas}+N_{\rm Al})$ in an obvious notation.

In Sec. V, we describe a measurement of f for Ar at 7150 Torr. The result is $f=0.3$ for forward decays, $f=0.45$ for backward decays.

We averaged the signal in Eq. (36), using $b_0/2\pi = 7.4$ MHz, $\tau=0.23$ μsec, and obtained for the peak signal

$$\langle S_0\rangle = 0.51\ (\tfrac{1}{3})(\tfrac{1}{2})(0.55)f = 0.047f. \qquad (38)$$

We thus predict a peak signal of 1.4% for forward decays, 2.5% for backward decays. We observed 1.4(2)% and 2.2(2)%, respectively.

III. APPARATUS

The major elements of the apparatus were (a) the microwave cavity; (b) a system for generating and phase-shifting two fast high-power microwave pulses; (c) a magnetic shielding system; (d) the target pressure vessel; (e) a gas circulating and purifying system; (f) a scintillation counter telescope to detect muons stopping in the pressure vessel, and their associated decay positrons; (g) proportional counters inside each end of the pressure vessel, to confine accepted muon stops to the actual cavity; (h) logic circuitry to form the appropriate stop and decay signatures, and to trigger the microwave system; (i) digitron timing, scaler, and data retrieval system for timing the muon decay.

Elements d–i were similar to those in previous experiments,[1,2] so that only those features which were new or different will be emphasized in what follows.

A. Microwave Cavity

Figure 4 shows a detailed view of the microwave cavity. The cavity was an aluminum cylinder, 30 cm long × 31.750(12) cm diam × 1.6 cm thick, which resonated near 4463 MHz in the TM_{050} mode.

In designing the cavity and choosing the mode to be used, three criteria were important: First, the mode should be isolated as far as possible from adjacent modes. Second, its power distribution should have minimum variation over the cavity volume. Third, the cavity diameter should be as large as practical to minimize wall stops. These criteria are approximately optimized by the choice of the TM_{050} mode. Its nearest neighbors are TM_{721} at ~9 MHz lower, and TE_{342} at ~20 MHz higher frequency. The field distribution in the cavity gives an optimum signal which is 51% of that for a hypothetical homogeneous rf field, as

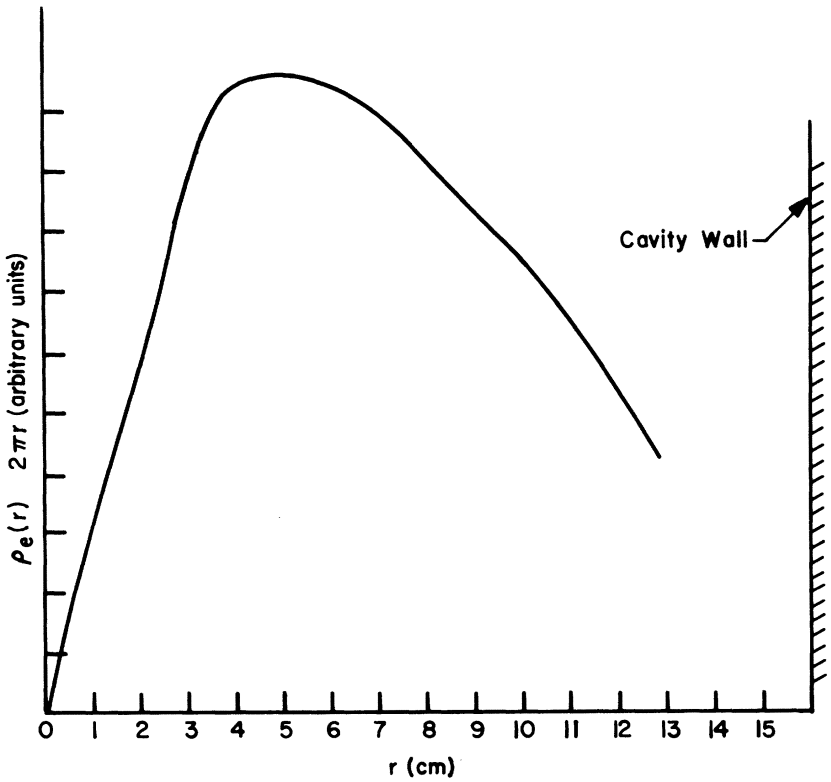

FIG. 3. Distribution ρ_e of decay positrons in the cavity.

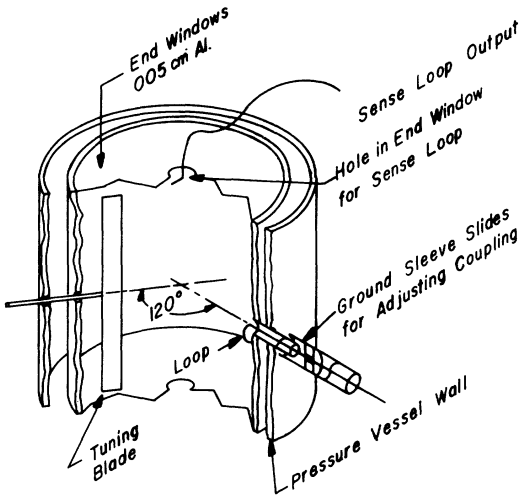

FIG. 4. Detail of the microwave cavity, showing coupling loop and sense loop.

discussed in Sec. II E. Further increasing the cavity diameter would have decreased the mode spacing rapidly, and made it impossible to satisfy the first criterion.

The length of the cavity is arbitrary for the TM_{050} mode, since the field is z independent. The choice of 30 cm length maximizes $\rho_e \langle \cos\theta \rangle$ averaged over the interior of the cavity, and gives maximum separation of TM_{050} from neighboring modes.

The TM_{050} resonance frequency was tuned to the frequency of the exciting field by means of a polystyrene blade, $28 \times 2.5 \times 0.3$ cm, suspended axially within the cavity. This blade could be moved radially by a quartz rod which extended outward through the cavity and pressure vessel, and tuned the resonance through a 500 kHz range. The gas in the cavity caused a dielectric shift of the resonance, which varied in magnitude according to the gas conditions (e.g., Ar at 7150 Torr or Kr at 2720 Torr). We compensated for these variations by placing polystyrene rings, of 31.7 cm o.d. $\times$ 25 cm i.d. and thickness selected for each gas condition, near each end of the cavity.

We determined the Q of the cavity by measuring the width of the TM_{050} resonance: $Q = \omega_0/\Gamma_c$, where Γ_c is the FWHM of the cavity resonance. The unloaded Q of the empty cavity was 40 000. The unloaded Q of the cavity with polystyrene tuning rings is given in Table I for each gas condition used in the experiment. The loaded Q_L was 4000 in all cases.

The fractional thermal expansion of the aluminum walls is $\sim 25 \times 10^{-6}/°C$, giving a tuning shift of ~10 kHz/°C. Since this is only $0.1\Gamma_c/°C$, no significant tuning deviations resulted.

We apply a square rf pulse with power P_i, length τ, frequency ω_0, to the cavity. The field inside the cavity responds with a time constant $\tau_c = 2Q_L/\omega_0$:

$$B_1 = B_0(1 - e^{-t/\tau_c}), \quad 0 < t < \tau \tag{39}$$

$$= B_1(\tau) e^{-(t-\tau)/\tau_c}, \quad \tau < t. \tag{40}$$

The efficiency of coupling the field into the cavity within a time 2τ is maximum for $\tau \simeq \tau_c$. We thus wanted the cavity to have $Q_L \simeq \frac{1}{2}\omega_0\tau = 3200$; since the unloaded Q of the cavity was more than ten times greater, we reduced Q_L by overcoupling the cavity input.

The rf field was coupled into the cavity by a rectangular loop of copper strip (5-cm^2 enclosed area, 10-cm perimeter) which connected the center conductor of the input coaxial structure to the cavity wall. The coupling loop acts as an ideal transformer in coupling the microwave transmission line to the cavity. The "turns ratio" x corresponds to the strength of coupling. Resistive losses R_0 in the cavity walls appear as a load $R = x^2 R_0$ to an input transmission line, whose characteristic impedance is $Z_0 = 50\Omega$. The magnitude of x is chosen empirically by appropriately shaping the coupling loop. The input is matched to the cavity when $Z_0 = R$. If one overcouples to the cavity, part of the incident wave reflects from the input. If the incident wave in the transmission line has amplitude V_i, the amplitude across the load is[17] $V_L = 2V_i R/(R + Z_0)$. The

TABLE I. Rates (sec^{-1}) and other information for each data run.

Gas	Running time (days)	Unloaded cavity Q	μ	S	Total Se_B	Total Se_F	$t > T + 2\tau$ Se_B	$t > T + 2\tau$ Se_F	Accidentals[a] α_B	Accidentals[a] α_F
2742 Torr Kr	14	14 400	340	165	10	9	1.1	1.5	0.05	0.02
6469 Torr Kr	3	23 200	1250	720	56	49	6.4	6.3	0.05	0.02
7150 Torr Ar	4	18 800	1130	550	36	44	4.7	5.9	0.05	0.02

[a] The accidentals α are defined in Appendix A.

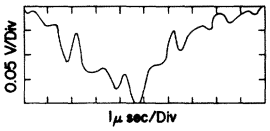

FIG. 5. Sense-loop response. Significant features are the rise time τ_c = 280 nsec, and the beat pattern due to $\omega_a \neq \omega_c$.

loaded Q of the cavity is $Q_L = QZ_0/(R+Z_0)$, and the power transmitted to the cavity is then

$$P_L = P_i(V_L^2/R)/(V_i^2/Z_0)$$

$$= 4P_i Z_0 R/(R+Z_0)^2 \simeq 4P_i Q_L/Q . \quad (41)$$

The power dissipated in the cavity is

$$P_c = (\omega_0/8\pi Q)\int B_1^2(r)d^3r .$$

We calculated this integral using Eq. (34) for $B_1(r)$, with $b_0/2\pi(\mathrm{MHz}) = 0.7B_{10}(\mathrm{G})$. We obtained

$$P_c = 0.086\omega_b(b_0/2\pi)^2 V_c/8\pi Q , \quad (42)$$

where $V_c \simeq 24l$ is the cavity volume. Requiring $P_L = P_c$, we relate the input power to b_0. We used $Q_L = 4000$ throughout the experiment, so

$$P_i(\mathrm{W}) = 14.8[b_0/2\pi(\mathrm{MHz})]^2 . \quad (43)$$

With the available input power (810 W) we generate $b_0/2\pi = 7.4$ MHz inside the cavity.

We inserted a sense loop near a hole provided at the center of the downstream cavity window for gas flow (see Fig. 4). Since the on-axis position of this loop makes it sensitive only to modes with nonzero fields at $r = 0$, it acts as a strong selector for the TM_{050} mode. We monitored the power pulse through this loop with a fast diode detector (Microlab FXR XP-20), and could thus observe the time structure of the rf field in the cavity (see Fig. 5).

B. Microwave Pulsing Network

Figure 6 is a diagram of the microwave network. A thermostatted quartz crystal oscillator (International OT-61), at frequency ≃93 MHz, drives a frequency multiplier (Varian 25C9620C) which generates a 16th and 48th harmonic. The 16th harmonic is counted by a frequency counter (HP5245L), which is stable and calibrated to 1 part in 10^8. The 48th harmonic passes through a circulator isolator and into the phase-shifting network.

This network contains a circulator, a SPST microwave switch (AEL SNB181A), and an adjustable-length shorted stub. The circulator routes the power from the oscillator multiplier to the switch. The $\varphi = \pm\frac{1}{2}\pi$ phase shift is produced by phase-shifting either the first or second pulse by $\frac{1}{2}\pi$. If no phase shift is desired, the switch is closed; the power reflects from the switch and the circulator then routes it to the TWT input. If the switch is open, the power goes down the shorted stub and is reflected back through the

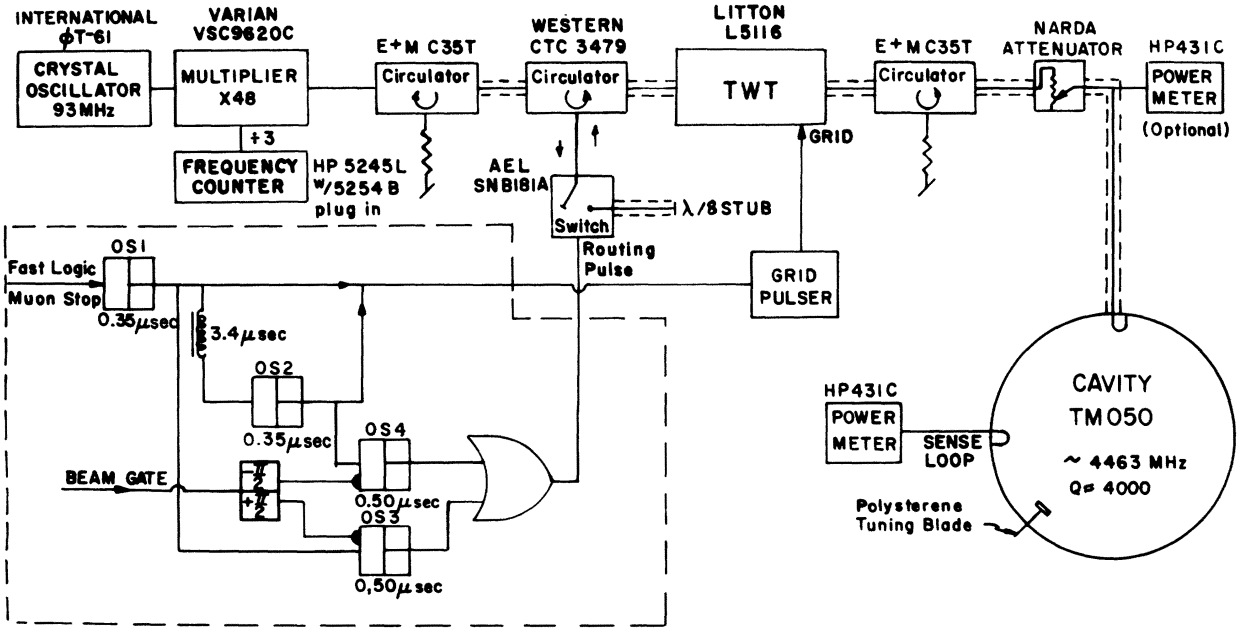

FIG. 6. Microwave network. First pulse of a pair is fired by 0S1 and shifted by 0S3; second pulse is fired by 0S2 and shifted by 0S4. 3.4 μsec delay between 0S1 and 0S2 is $(T+\tau)$ as defined in the text.

switch and on to the TWT. The length of the stub was chosen ($\frac{1}{8}\lambda$) so that the two switch positions produce a relative phase shift of $\frac{1}{2}\pi$. There was a finite attenuation in the extra path length in the open-switch position, so that the power delivered to the TWT input was different by ~1 dB for $\varphi = \frac{1}{2}\pi$. Figure 7 includes the timing sequence of the rf power pulses and phase shift for $\varphi = \frac{1}{2}\pi$.

The microwave power pulse was generated by a grid-controlled traveling wave tube (Litton L-5116). The TWT was held off by a grid bias (−140 V), and turned on by pulsing the grid positive (+70 V) for time τ. The pulse separation $T + \tau$ was controlled by the fixed delay between two one-shots (0S1 and 0S2 in Fig. 6), and was set at 3.4 μsec for all our data. The pulse length τ was adjustable from 0.2 to 0.6 μsec on the grid pulse driver, and was the same for both pulses. The TWT output power during the experiment was 1070 W; the power delivered at the cavity input was 810 W.

C. Magnetic Shielding

The magnetic field in the cyclotron experimental area was ≃10 G. We achieved a shielding factor of $>10^3$ over the entire cavity volume using the arrangement shown in Fig. 2. The shielding array consisted of three concentric cylinders, and was similar to that of the Yale group.[3] It was designed to maximize the shielding factor at its center for a given amount of shielding material.[18] The cylinders were fabricated from 150 lb of Allegheny-Ludlum Moly-Permalloy ($\mu \simeq 40\,000$), and hydrogen annealed.

Without end caps such an array cannot effectively shield against a longitudinal (axial) field component. The requirement of a low momentum μ^+ beam entering the upstream end precluded a cap there, while a cap downstream would have been awkward for connecting and servicing the apparatus within. We chose to mount a pair of correction coils on the inner face of the innermost shield, each 25 cm from the median plane (see Fig. 2). The optimum current (70 mA) in the coils was determined by using a 1-mG sensitivity flux-gate magnetometer (HP 428B) to map the field in the region of interest. The field map (Fig. 8) indicates that the residual field did not exceed 5 mG transverse, 10 mG longitudinal over the cavity volume.

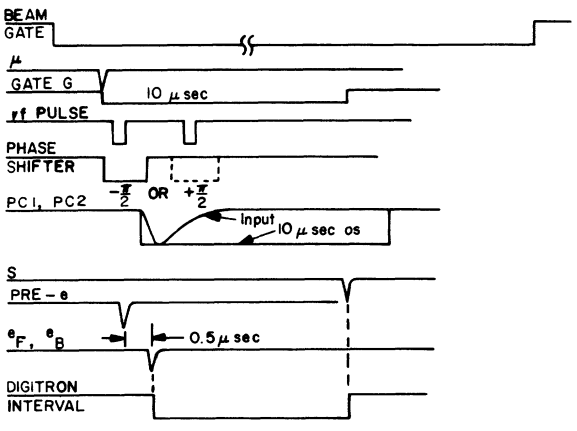

FIG. 7. Timing diagram. The phase-shift network is pulsed during one of the two rf pulses in each pair, as indicated.

D. Pressure Vessel

The pressure vessel was made of 40 cm diam, 0.6 cm thick No. 304 stainless-steel pipe, with 2.5×3.8 cm cross-section flanges on the ends. The end windows were of Alclad sheet, hydroformed to a spherical cap (90 cm radius), and secured to the end flanges by mating 2.5×3.8 cm rings. A step groove eliminated slippage, and a Viton *O*-ring formed a pressure-vacuum seal.

To mimimize background from muons stopping in the windows, we used the thinnest windows which were safe (each window was hydrostatically tested to twice the operating pressure). For the high-pressure Ar and Kr data, we used 0.050 cm thickness; for the low-pressure Kr data, 0.025 cm.

E. Gas Purifying System

Impurities can depolarize muonium when present in few ppm concentrations,[19] so that continuous purification of the buffer gas is required. The gas purifying system was improved over that of Refs.

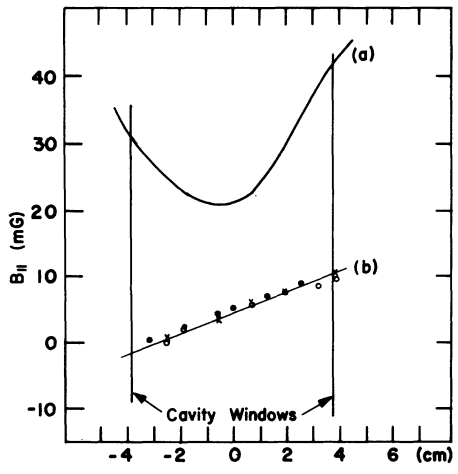

FIG. 8. Map of remanent longitudinal-field distribution: (a) without correction coils, $r = 7.5$ cm; (b) optimum current (70 mV) in correction coils; ○, $r = 5$ cm; ×, $r = 10$ cm; ●, $r = 12.5$ cm.

1 and 2, and is illustrated in Fig. 9. All components were of No. 304 stainless steel, and whenever feasible metal-metal seals were made at joints. Under vacuum, the combined leak and outgasing rate was typically 5×10^{-4} std cm^3/sec; the total volume of the system including the pressure vessel was 55 l.

We will trace the gas flow starting at the exit of the pressure vessel. It first passed through a high-pressure piston pump (Whitey LP-10), which forced a 1.6 cm^3/sec volume flow. It then entered the oven, flowing up through an outer region of radiative heat shields and then down through a 2.5-cm-diam ceramic pipe which contained three tantalum baskets filled with activated titanium sponge (Johnson Matthey Chemicals Ltd.). This pipe was electrically heated to 900 °C, at which temperature the titanium exhibits optimum chemical activity.[20] The oven temperature was controlled by feedback from thermocouples inserted into the tantalum baskets, and calibrated with an optical pyrometer which looked directly at the titanium through a quartz window at the top of the oven assembly.

The gas was then cooled in a water-jacket column and a coil immersed in a dry ice-acetone slush, which also served to freeze out condensibles. The gas flow was measured with a calibrated ball gauge, and the pressure with a quartz Bourdon tube manometer (Texas Instruments 141A), calibrated to ±5 Torr. The reference of this meter was maintained in vacuum, so that it read absolute pressure directly. The gas temperature was monitored by three thermistors located inside the pressure vessel (but outside the cavity to avoid rf heating); the resulting temperature measurement was calibrated and reproducible to ±0.5 °C.

The final element in the system was a cylindrical proportional counter. An α source (Cm^{242}) on the tip of a glass rod was mounted close to its center wire. We found empirically that the pulse-height spectrum of the counter was sensitive to the presence of those impurities which affected the signal height in the muonium experiment. This counter served as a rough indicator of gas purity, and on several occasions forewarned of intolerable impurity levels.

Within the pressure vessel the clean gas entered the rf cavity directly through the microwave input, and left the cavity through holes in the centers of its end windows.

The gas system allowed for evacuating all parts including the pressure vessel before filling with the buffer gas. To avoid implosions, heavy domes were fitted from the outside over the thin pressure vessel end windows and evacuated. Low impedance 2.5-cm-diam lines connected directly from the diffusion pump column to the oven assembly and the pressure vessel, allowing evacuation to $<10^{-4}$ Torr in 20 min. Back flow of vacuum-pump oil was prevented by a cold baffle and a molecular sieve.

F. Scintillation Counters

The scintillation-counter telescopes shown in Fig. 2 were essentially as in our previous exper-

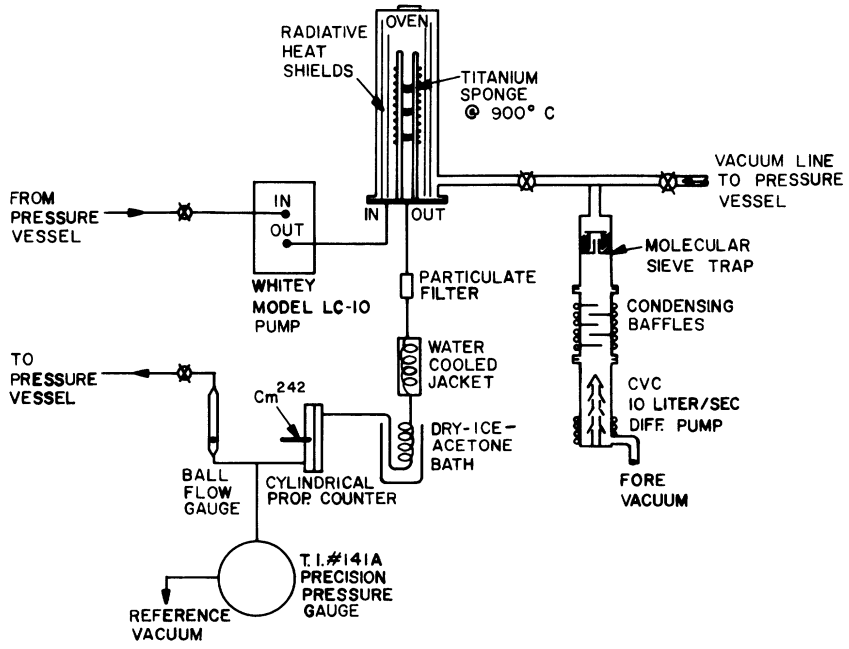

FIG. 9. Gas-purifying system. Vacuum column is valved off during normal operation.

ments.[1,2] Counters 2, 3, 5, and 6 were 33 cm diam×0.3 cm thick NE110 scintillant. Counter 1, 20×20×0.3 cm was located upstream of the collimator and moderator. It served as a beam monitor, and as a prompt veto in the decay positron signatures. Counter 4 was 12 cm diam×0.6 cm thick, and served as a collimation counter in the muon stop telescope. We also used 4 for pulse-height discrimination between slow muons and fast positrons.

G. Proportional Counters

In all of our muonium experiments,[1,2] we used multiwire proportional counters (PC) to (a) exclude muons stopping in the pressure vessel windows, and (b) discriminate between muons and positrons. PC1 and PC2 were situated inside the pressure vessel as shown in Fig. 2. The construction of the PC's is detailed in Fig. 6 of Ref. 1. The upstream counter PC1 had a restricted sensitive area of 12 cm diam, obtained by sandwiching a Mylar film annulus on each side of the anode plane. PC1 thereby effectively collimated the incident beam in conjunction with counter 4. The downstream counter PC2 had a 30-cm-diam sensitive area. Each counter had a mass of 4 mg/cm^2, which is negligible in comparison with the mass of the gas in the cavity for even the low-pressure Kr data (500 mg/cm^2).

The output from each proportional counter was amplified by a charge-sensitive amplifier with FET input, and pulse-height discriminated before being used in the muon stop signature. The efficiencies of the PC's for muons (ϵ_μ) and positrons (ϵ_e) were measured as in Ref. 1, and were typically $\epsilon_\mu = 0.85$, $\epsilon_e = 0.15$, corresponding to a discrimination factor $\epsilon_\mu/\epsilon_e = 5.5$. Note that the inefficiency of PC2 for muons leads to a contamination from muons stopping in the downstream pressure vessel window, and acts as a nonmuonium background just as do stops in the cavity walls.

H. Detection Logic

Figure 10 is a schematic of the detection logic used in the present experiment. The relative timing of the various logic pulses is displayed in Fig. 7.

Before each beam burst from the cyclotron, a pulse was sent to the logic, where it opened a 0.8-msec long gate B ("beam gate") covering the duration of the beam spill (0.5 msec). The repetition rate of the "stochastic" cyclotron pulses

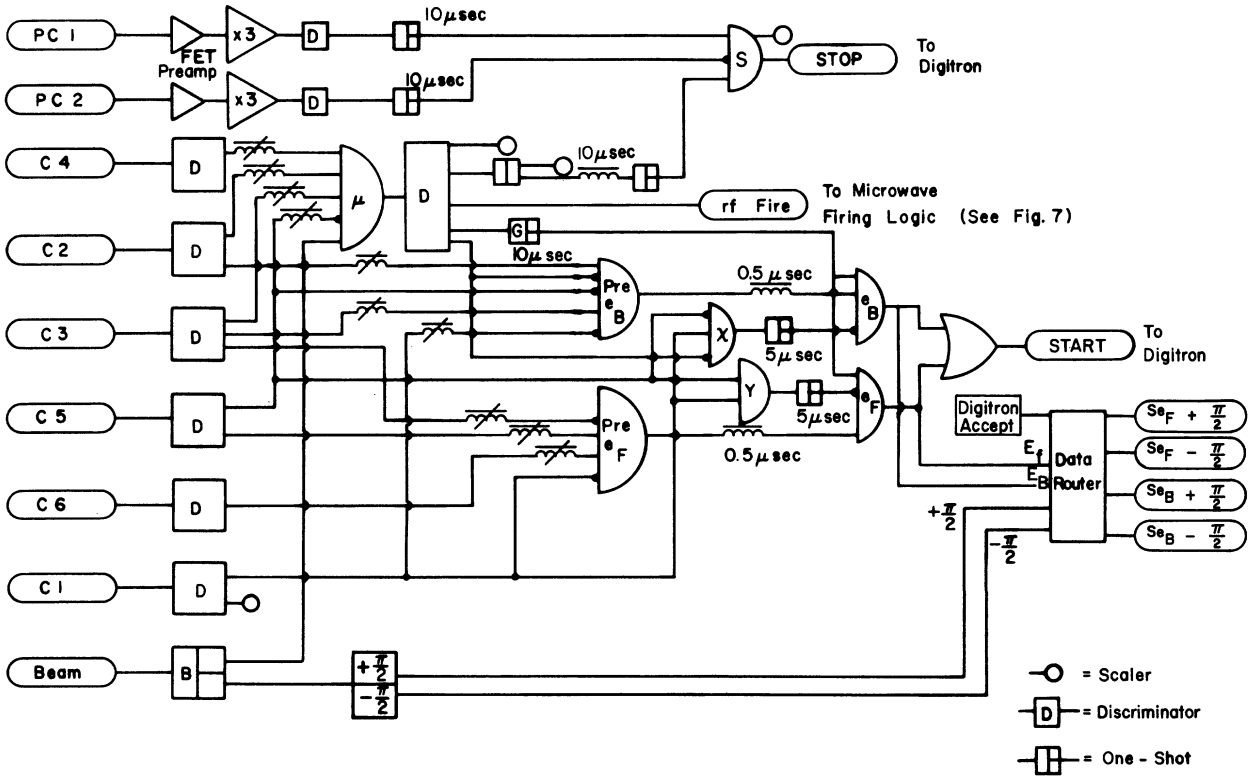

FIG. 10. Logic network. Widths and delays for forming S are indicated; Se events require a valid timing sequence in digitron, signaled by DIGITRON ACCEPT. The $\varphi = \pm\frac{1}{2}\pi$ routing alternates with each beam pulse.

was ~1 kHz. The beam gate entered the muon stop signature and triggered a flip-flop which changed the phase shift of the rf pulse pattern between $\pm\frac{1}{2}\pi$ on alternate beam pulses (see Fig. 6).

A muon stopping in the pressure vessel generated a signature $\mu = (2 \cdot 3 \cdot 4 \cdot \bar{5} \cdot B)$, and opened a 10 μsec gate G, defining $t = 0$. Decay positrons triggered a signature pre-$e_F = (5 \cdot 6 \cdot \bar{3} \cdot \bar{1})$ for a forward decay or pre-$e_B = (2 \cdot 3 \cdot \bar{5} \cdot \bar{1} \cdot \bar{\mu})$ for a backward decay. The pre-e signatures were delayed by $\delta_1 = 0.5$ μsec before forming a coincidence with G, thus allowing a measurement of the accidental background from events with $t<0$. This accidental background results in a time-independent event rate underneath the exponential muon decay in the time spectrum.

The salient difference between the logic of Fig. 10 and that used by us earlier (Fig. 3 of Ref. 1), aside from the rf triggering, was the addition of the X and Y coincidences to the decay signatures. The function of these circuits was to reduce the rate of accidental μ-e coincidence from muons stopping outside the pressure vessel. In the backward-decay telescope, such events correspond to muons traversing counter 1 and stopping in the collimator or moderator without producing a μ signature. The decay positrons from these muons can form a valid pre-e_B signature and make accidental coincidences with a legitimate μ signature. We formed the signature $X = (1 \cdot \bar{5} \cdot \mu)$ and generated a blocking gate of width T_x. The final backward-decay signature was then $e_B = (2 \cdot 3 \cdot \bar{5} \cdot \bar{1} \cdot \bar{\mu}) \cdot G \cdot \bar{X}$. Figure 11 shows the $t<0$ accidentals rate as a function of T_x. Two thirds of the accidentals show an exponential decrease with a characteristic time of 2.2 μsec, and are thus susceptible to $\bar{X}$ rejection. We used $T_x = 5$ μsec, thereby reducing the backward accidentals rate by a factor 2 with no significant loss in legitimate coincidence rate.

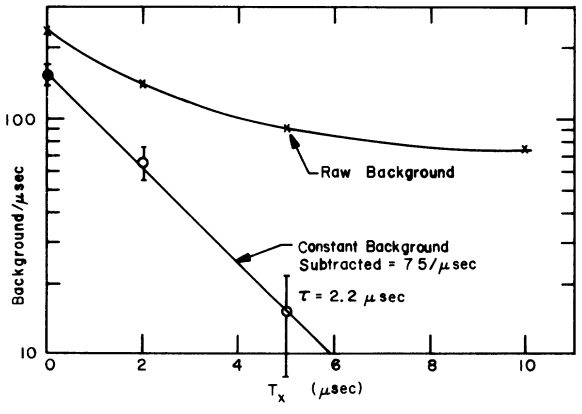

FIG. 11. X-circuit background rejection. The exponential T_x dependence shows that $\frac{2}{3}$ of backwards accidentals are X-related.

We added a similar circuit in the forward-decay signature, to protect against decays from muons stopping in counters 5 and 6. We formed the signature $Y = (1 \cdot 5)$ and generated a 5 μsec blocking gate. The final forward decay signature was $e_F(5 \cdot 6 \cdot \bar{3} \cdot \bar{1} \cdot) \cdot G \cdot \bar{Y}$.

We formed a coincidence between μ and the two PC's in order to accept only muons stopping in the actual cavity. Since the PC's operated in an ultra-pure noble gas in the absence of quenching agents, and at several atmospheres pressure, they gave pulses with rather poorly defined shape and timing.[1] To avoid ambiguities in timing, we delayed the μ signature by $\delta = 10$ μsec and shaped the PC outputs to form 10-μsec-long logic pulses. We then formed the "super-stop" signature $S = [(\mu)_\delta \cdot \mathrm{PC1} \cdot \overline{\mathrm{PC2}}]$.

The digitron,[1,21] a 10-MHz digital interval timer, measured the delay between a μ stop and a decay e^+. The timing interval is started by a fast e^+ signature and stopped by S (10 μsec *after* the μ signature signaling a muon stop). The decay positron rates are ~20% of the fast muon stop rate. The inverted e-μ timing starts the timing sequence only for events where a decay was observed.

A decay positron which forms a valid e-μ timing sequence in digitron is termed a superpositron S_e. Each superpositron event was stored in a 4×100 channel array. The digitron timing interval defines an address range 1–100, and the decay direction and rf phase shift define one of four data fields.

IV. SYSTEMATICS CONSIDERATIONS

Several effects complicate in practice the idealized situation described in Sec. II. We will discuss them here, and examine their effects as far as possible analytically. The question of any systematic offset of the zero crossing of $S_2(\Delta)$ is of particular interest.

A. TWT Frequency Shifts

The TWT output suffers a phase change (relative to the input) of $d\varphi/dV = -0.3°/\mathrm{V}$ for changes in the cathode voltage $V \simeq 10$ kv. This is a direct result of the change in electron transit time through the tube.[22] During the rf pulse, we observed a cathode voltage sag of 20 V, which is consistent with the 0.02 μF capacitance of the charging circuit. The cathode current during a grid pulse was 1.2 A, so that $dV/dt = I/C = 55$ V/μsec. This corresponds to a phase shift rate, i.e., frequency shift, of $\delta\omega = (0.0052 \text{ rad/V})(55 \text{ V}/\mu\text{sec}) = 0.30$ Mrad/sec

(45 kHz), between the frequency ω_a applied to the cavity and the free-running oscillator frequency ω_f.

A second source of frequency shift arises from dynamic effects in the TWT pulse operation. When the grid is pulsed, the phase of the output wave has a time structure due to the finite time involved in stabilizing the electron beam in the tube; a similar structure occurs when the grid is turned off. The resulting frequency shifts vary during the pulse, reaching a maximum of ~0.8 MHz. The beam pattern due to these frequency offsets is evident in the actual cavity pulse reproduced in Fig. 5.

The frequency difference $\Delta_a \equiv \omega_0 - \omega_a$ determines the extent to which the rf field can induce the muonium transitions of the split-field resonance $a = +[\Delta_a^2 + (2b)^2]^{1/2}$ in Eq. (14). But only the phase difference $\Delta_f(T+\tau) + \varphi$ determines the final polarization ($\Delta_f \equiv \omega_0 - \omega_f$), and nowhere in the time evolution equations do we require $\omega_a = \omega_f$. Hence no zero crossing offset can occur in $S_2(\Delta)$. A distortion of the actual line shape does occur, since the frequency ω_a at resonance is no longer at the peak of the $(2b/a)^2$ envelope. The linewidth of this Lorentzian envelope at our power level is ~2.5 MHz. The frequency ω_a is also offset from the cavity resonance (width $\simeq$1.1 MHz).

B. TWT Phase Shift

After the first pulse, the cathode charging capacitor is recharged through a series resistance of 15Ω, owing to overload protection fuses. The cathode voltage thus recovers with an RC time constant of 0.3 μsec, leaving a remnant phase shift at the beginning of the second pulse of $\delta\varphi = (20V)\,(-0.3°/\mathrm{V})e^{-11} = -6\times10^{-5}°$. A rather involved measurement, described in Sec. V shows no phase shift to with ±1°.

The signal with a phase shift $\delta\varphi$ on the second pulse is

$$S_2(\Delta) = S_0 \sin[\Delta_f(T+\tau) + \delta\varphi].$$

A zero-crossing offset occurs: $\delta(\Delta\nu) = \delta\varphi/(T+\tau)$ = 0.3 rad/sec (0.05 Hz). The limit of measurement of $\delta\phi$ corresponds to an offset of 800 Hz = 0.2 ppm.

C. Microwave Pulse Shape

The field inside the cavity is a superposition of the applied field $b\cos\omega_a t$ and an induced transient $-be^{-t/\tau_c}\cos\omega_c t$ at the cavity resonant frequency ω_c [with $\omega_c = \omega_a$, we have Eq. (39)]. Dropping counterresonant terms as before, the effective field exciting the muonium atom is

$$B_1(t) = \tfrac{1}{2}B_1(e^{-i\omega_a t} - e^{-t/\tau_c}e^{-i\omega_c t}),\quad 0<t<\tau \qquad (44)$$

where $\tau_c = 2Q_L/\omega_c$. With $Q_L = 4000$, $\tau_c = 0.28$ μsec.

At the end of the pulse ($t = \tau$) when the applied field is turned off, a second transient is induced in the cavity, with initial phase and amplitude to match the field $B_1(\tau)$:

$$B_1(t) = B_1(\tau)e^{-(t-\tau)/\tau_c}e^{-i\omega_c(t-\tau)},\quad \tau<t. \qquad (45)$$

Similar transients are induced by the second pulse. These transients make the time evolution equations insoluble in closed form, so that the latter must be integrated numerically. We find no zero crossing shift at the level of one Hz for $|\omega_0 - \omega_a| \leq 6$ Mrad/sec (1 MHz). The cavity mode was tuned to the frequency of the applied field with an error of ±150 kHz.

D. Unequal Pulse Length and Duration

We wish to examine the effect on the amplitudes $A_i(t)$ if $b_1 \neq b_2$, $\tau_1 \neq \tau_2$ for two square rf pulses. Defining $F_i = F(b_i\tau_i)$, $G_i = G(b_i\tau_i)$, we have

$$P_z(T+\tau_1+\tau_2) = \mathrm{Re}[e^{i\Delta(\tau_1+\tau_2)/2}F_1F_2 + e^{i\Delta(T+\tau_1)+i\varphi}G_2]. \qquad (46)$$

Even if $F_1, F_2 \neq 0$, the first term does not depend on φ, and hence cannot contribute to the signal. Since G is pure imaginary for all b, τ,

$$S(\Delta) = S_0 \sin b_1\tau_1 \sin b_2\tau_2 \sin\Delta(T+\tau_1). \qquad (47)$$

Hence no zero-crossing offset can arise from this source, even for phase-shift-correlated differences in b, τ.

There was a ~1-dB attenuation between the input powers to the TWT with and without phase shift. With the TWT operated as far into saturation as the available input power permitted, this produced a relative attenuation of 0.5 dB(12%) on the TWT output. The corresponding field attenuation is 6%. The resulting signal height in Eq. (47) is reduced by 0.5%.

E. Static Magnetic Fields

We described the magnetic-shielding arrangement in Sec. III C. The remnant fields did not exceed 5 mG transverse, 10 mg longitudinal over the cavity volume. We now consider the effect of weak static fields on the amplitudes $A_i(t)$.

A transverse field $B_\perp$ mixes the (1, ±1) states with the (1, 0) state by applying a perturbation tending to change the axis of quantization. The equations of motion become

$$\begin{aligned} i\dot{A}_- &= be^{i\Delta t}A_{00},\quad i\dot{A}_{00} = be^{-i\Delta t}A_-,\\ i\dot{A}_+ &= b_\perp A_{10},\quad i\dot{A}_{10} = b_\perp A_+, \end{aligned} \qquad (48)$$

where $\hbar b_\perp = (g_s + g_\mu')\mu_B B_\perp/2\sqrt{2}$. In convenient units, $b_\perp/2\pi(\mathrm{MHz}) = 1.0B_\perp(\mathrm{G})$. The motion of the ampli-

tudes A_-, A_{00} are again described by Eq. (13). The motion of A_+, A_{10} has the solution

$$\sqrt{2}A_+ = \cos b_\perp t\,, \quad \sqrt{2}A_{10} = \sin b_\perp t\,. \tag{49}$$

The resulting polarization for $\frac{1}{2}\pi$ pulses is

$$P_z(T+2\tau) = \cos b_\perp(T+2\tau)\cos[\Delta(T+\tau)+\varphi]\,. \tag{50}$$

No zero crossing offset is produced. The effect on the peak signal height of a 5-mG transverse field is 0.5%.

A longitudinal field $B_\parallel$ breaks the degeneracy of the $F=1$ states. The resulting equations of motion are

$$\begin{aligned} &i\dot{A}_- = b_\parallel A_+ + be^{i\Delta t}A_{00}\,, \quad i\dot{A}_{00} = be^{-i\Delta t}A_-\,,\\ &i\dot{A}_+ = b_\parallel A_-\,, \quad iA_{10} = 0\,,\\ &\hbar\, b_\parallel = (g_s + g_\mu')\mu_B B_\parallel/2\sqrt{2}\,. \end{aligned} \tag{51}$$

The A_-, A_+, A_{00} system does not admit closed form solution. We can test for the presence of a zero crossing offset by requiring $\Delta = 0$. Eq. (51) becomes

$$i\dot{A}_- = bA_+ + bA_{00}\,, \quad i\dot{A}_+ = bA_-\,, \quad i\dot{A}_{00} = bA_-\,. \tag{52}$$

The solutions are

$$\begin{aligned} &\sqrt{2}A_- = \cos b't - \alpha_\parallel i\,\sin b't\,,\\ &\sqrt{2}A_+ = \alpha_\parallel^2\cos b't - \alpha_\parallel i\,\sin b't + \alpha_0^2\,,\\ &\sqrt{2}A_{10} = \alpha_0\alpha_\parallel\cos b't - \alpha_0 i\,\sin b't - \alpha_0\alpha_\parallel\,, \end{aligned} \tag{53}$$

where

$$b'^2 = b_\parallel^2 + b^2\,, \quad \alpha_0 = b/b'\,, \quad \alpha_\parallel = b_\parallel/b'\,.$$

With $t=\tau$, this gives the amplitudes after the first pulse. For $\varphi = \pm\frac{1}{2}\pi$ at the beginning of the second pulse, the equations of motion become

$$i\dot{A}_- = bA_+ \pm ibA_{00}\,, \quad iA_+ = bA_-\,, \quad iA_{00} = \mp ibA_-\,. \tag{54}$$

The solutions are the same as Eq. (52) except $A_{00} = \pm iA_{00}$. Hence the final polarization is φ independent and can give no zero-crossing offset.

F. Non-$\frac{1}{2}$ Phase Shift

If the relative phase φ of the shifted and unshifted pulses is not $\frac{1}{2}\pi$, Eq. (21) becomes

$$S(\Delta) = S_0(2b/a)^2\sin\varphi\sin\Delta(T+\tau)\,. \tag{55}$$

Again no zero crossing offset is possible, and a small reduction in signal results; for a phase-shift error of $\pm5^\circ$ (see Sec. V) the signal is reduced by 0.5%.

G. Numerical Analysis of Systematics

The preceding arguments on the effects of external static fields and of frequency modulation are given for the analytically soluble case of square pulses. Since the rise and fall times of the TWT and the transient behavior of the cavity result in considerable amplitude and frequency modulation, one was perhaps left uncertain as to the validity of those arguments. We therefore proceeded to calculate the signal numerically under several typical running conditions.

The equations of motion for an arbitrary time-dependent rf driving field $b(t)$ are

$$\begin{aligned} &i\dot{A}_- = b_\parallel A_+ + b(t)A_{00}\,,\\ &i\dot{A}_+ = b_\parallel A_- + b_\perp A_{10}\,,\\ &i\dot{A}_{10} = -b_\perp A_+\,,\\ &i\dot{A}_{00} = b^*(t)A_-\,. \end{aligned} \tag{56}$$

We evolved $A_i(t)$ incrementally using $\dot{A}_i$ and $\tilde{A}_i$, through the double-pulse rf field of Eqs. (44) and (45). We allowed for a TWT frequency offset of the driving field ($\omega_a \neq \omega_f$), and for tuning errors ($\omega_c \neq \omega_f$). Effects of the small (residual) static fields $b_\parallel$, $b_\perp$ were also included. Using Eq. (15), we then calculated the signal $S(\Delta)$ at each point in the cavity, using the amplitudes A_-, A_+ after the second pulse. We next averaged that signal over the cavity volume as in Eq. (36), weighting with the distributions ρ_e, $\langle\cos\theta\rangle$, and $\sin^2 b\tau$ (see Sec. II E).

The resulting single- and double-pulse resonance curves, calculated for the actual conditions of the experiment, are shown in Figs. 14 and 16, respectively. Both curves agree well with the experimental data. At the level of 1 Hz no zero-crossing shift is induced.

In addition to computing the signal under normal running conditions, we independently verified each of our analytically derived mechanisms regarding the separate effects of pulse amplitude, pulse frequency, and static field. We also investigated the effects (both individual and joint) of a range of variations of pulse shape, frequency, and static field beyond that encountered in a realistic experiment. Our findings are readily summarized; at a level of 1 Hz, no mechanism produced an offset of the zero crossing.

The shape of the resonance curve is affected in a manner which can be estimated from the analytic calculation. The combination of unequal pulse amplitudes with a frequency offset is interesting because the signal amplitude is diminished far more than would be expected from the separate effects of such variations. We stress that none of the effects considered shifts the zero crossing point, their sole effect being a reduction in signal height.

V. AUXILIARY MEASUREMENTS

Four kinds of auxiliary measurements were crucial to this experiment: (a) beam-range stud-

ies and stopping distributions; (b) attempts to veto muons stopping in the cavity walls; (c) a single-pulse experiment to determine the $\frac{1}{2}\pi$ pulse requirement; (d) microwave phase-shift measurements.

A. Beam Studies

We stop the beam in the buffer gas by inserting an appropriate amount of $(CH_2)_n$ moderator upstream. The optimum range brings the peak of the momentum distribution to rest in the gas. The stopping rate S and decay positron rate Se are plotted in Fig. 12 as a function of range. The equivalent thickness of the gas and the aluminum pressure vessel windows are superposed for the case of 2700-Torr Kr.

The distribution of stopping muons in the cavity is of considerable interest, since some muons end their life in the cavity walls, diluting the useful signal (see Sec. IIE). We wanted to measure the fraction f of muons stopping in the gas of the cavity. To do so, we produced a μ^- beam of the same momentum as our μ^+ beam by reversing the polarity of all magnets. To the extent that a low-energy μ^- slows down and scatters in the same way as a μ^+, the fraction stopping in the walls will be the same. The "decay rate" $1/\tau'_\mu$ for μ^- is the sum of rates for muon decay and nuclear capture, the latter being a strong function of the Z_{eff} of the nuclei in the environment[23]: $1/\tau'_\mu = \gamma + \Gamma_{\text{cap}} Z^4_{\text{eff}}$. For Al, $\tau'_\mu = 0.87$ μsec; for Ar, $\tau'_\mu = 0.45$ μsec. The decay time spectrum is thus a sum of two exponentials, and fitting for their zero-time intercepts yields f. Figure 13 shows a typical decay time spectrum; the fitted exponentials yield $f = N_{\text{gas}}/(N_{\text{gas}} + N_{\text{Al}}) = 0.3$ for Se_F, 0.45 for Se_B. As noted in Sec. IIE, the aluminum component included ~15% of the muons stopping in the downstream pressure vessel window, because of $\overline{\text{PC2}}$ inefficiency.

B. Wall Veto Attempts

We made two unsuccessful attempts to veto muons stopping in the cavity walls. The first was to line the inner cavity wall with a 0.3 cm thick cylindrical plastic scintillator. The light was guided out through slots in the downstream cavity window by strips of light pipe. Since these strips crossed the beam as they clustered, they were made of scintillator so they would self-veto. The system was necessarily optically inefficient, and worked only marginally.

In the second scheme, 25 anode wires of a proportional counter were located on a circle at the outermost zero of the rf field, 3 cm from the wall; the wall served as cathode. The wires actually

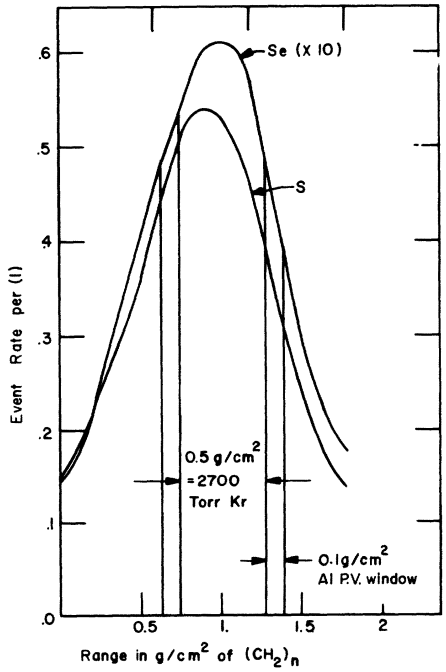

FIG. 12. Range curve for muons stopping in the cavity (S) and their associated decays (Se). The mass of the gas and of the pressure vessel windows correspond to the low-pressure Kr run.

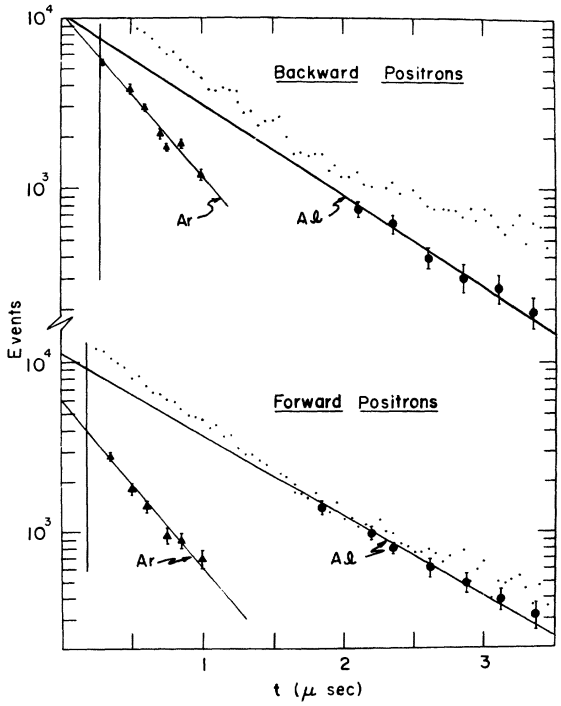

FIG. 13. Time dependence of μ^- decays (Se); the factor $f = N_{\text{gas}}/(N_{\text{gas}} + N_{\text{Al}})$ is obtained by a 2-exponential fit as shown.

improved the rf mode situation by acting as a strong selector for the desired TM_{050} mode.

This proportional counter, while being far from ideal, did have a reasonably uniform efficiency and energy resolution. Unfortunately, the volume of gas excluded by it was about half the total cavity volume, so that even perfect wall-stop rejection could give only a factor 1.3 greater statistical power in Se_F, and no improvement at all in Se_B. We finally abandoned this scheme as well, and accepted the wall-stop contamination as unavoidable.

C. Single-Pulse Resonance

We used a single-pulse resonance to determine the $\frac{1}{2}\pi$ pulse condition. The signal $\langle S_1(b_0\tau)\rangle$ is given by Eq. (37) for the case of a square rf pulse. We calculated S_1 numerically for the actual exponential rf pulse of Eqs. (44) and (45); Fig. 14 shows the result for $b_0/2\pi = 7.4$ MHz, as a function of pulse length τ. We find that maximum split-field peak signal (i.e., "$\frac{1}{2}\pi$ pulses" on the average) occurs at the value of τ where $S_1 = 0.6\, S_{10}$ (S_{10} is the peak signal for the single-pulse resonance): $\tau = 0.23\,\mu$sec. The single-pulse data are plotted in Fig. 14; we have insufficient statistics to resolve the damped oscillations of S_1, but do show good agreement with the calculated resonance in terms of the saturation signal and the coarse time structure of S_1.

D. Phase-Shift Measurement

We adjusted the $\frac{1}{8}\lambda$ stub of the phase-shifting network so that the shifted output waveform from the TWT had a phase of $\frac{1}{2}\pi$ relative to the unshifted waveform. The arrangement is shown in Fig. 15. The TWT output was strongly attenuated (~45 *dB*) and fed into one end of a slotted transmission line. A sample of the TWT input was fed into the other end, and a standing-wave pattern was produced.

We adjusted the two amplitudes to be equal using a variable attenuator, so as to maximize the interference. A maximum of the pattern was located with a diode detector, first with and then without phase shift. The distance d between maxima in the two conditions gives a shift $\varphi = 2\pi d/\lambda$. To achieve $\varphi = \frac{1}{2}\pi$, we adjusted the shifter stub length for a separation $d = \frac{1}{4}\lambda \simeq 1.7$ cm. Using this technique we could reproducibly set the phase shift to within ±5°.

To test for phase shift on the second pulse due to remnant cathode voltage sag (see Sec. IV B) we used the same arrangement as above. The standing wave pattern from the first and second pulse was displayed on an oscilloscope, and the slotted line probe adjusted to give maximum *dispersion* of the interference pattern (minimum peak amplitude). The sensitivity to a relative phase shift between the two pulses was ±1°. No shift was observed.

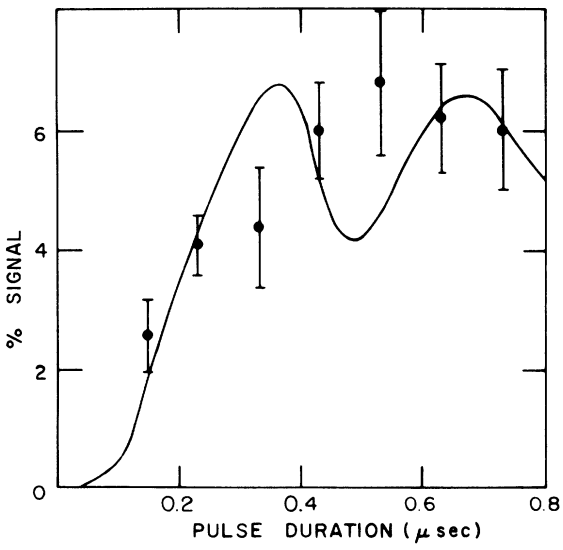

FIG. 14. Single-pulse resonance in 6469 Torr Kr. The curve is the computed resonance, taking into account all effects discussed in Secs. II E and IV. $\chi^2/N = 1.4$.

VI. ORGANIZATION OF THE EXPERIMENT

We wanted to extrapolate $\Delta\nu$ to zero pressure in two different gases. The statistically optimum use of running time dictates that data be taken at the lowest and highest possible pressures. The rate of muons stopping in the gas defined the low pressure limit; the high pressure was defined by the requirement of tuning the rf cavity to $\Delta\nu(P)$, and by the desire to minimize the effects of a quadratic pressure shift.[8]

We measured $\Delta\nu$ under three gas conditions: (i) Ar at 7150 Torr; (ii) Kr at 6469 Torr; and (iii) Kr at 2742 Torr.[24] In each resonance, we alternated

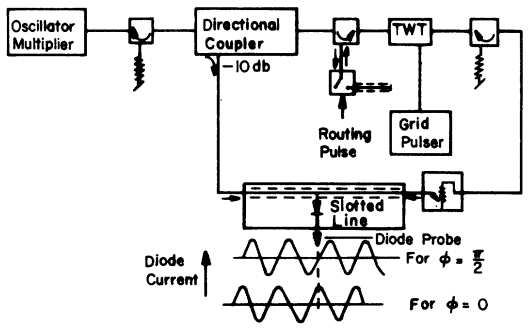

FIG. 15. Arrangement for phase-shift measurement. A change $\delta\varphi$ in the phase shift on TWT output causes a shift $\delta l = \lambda\delta\varphi/2\pi$ in the interference pattern on the slotted line.

signal runs on both sides of ω_0. In addition, we alternated the sequence of $\pm\frac{1}{2}\pi$ phase shifts with respect to each other and the beam pulse, in order to discover and possibly cancel any systematics of an instrumental origin. To examine the shape of $S(\Delta)$ and measure the maximum signal height $\langle S_0\rangle$, we spent ~10% of each resonance at or near the peaks of $S(\Delta)$.

Table I displays the muon stop and decay rates for the three gas conditions used in the experiment. During normal cyclotron operation, the beam monitor (counter 1) rate was $\sim 3\times 10^4$/sec. The prompt muon stop rate (μ) was about twice the superstop rate (S) for the high-pressure data, and $2.5S$ for the low-pressure Kr data. Note that the S/μ ratio is a direct measure of the reduction of background by the use of the proportional counters.

The total superpositron rate ($Se_f + Se_B$) was ~$0.25S$. This figure is consistent with the computed mean acceptance $\langle \Omega\cos\theta\rangle/4\pi = 0.15$ for each positron telescope.

VII. DATA ANALYSIS

For each gas condition, the data were used to compute the signal $S_2(\Delta)$ from which $\Delta\nu$ can be readily extracted. During individual runs we measured the following quantities: pressure p_i, temperature t_i, forward signal S_i^F, backward signal S_i^B, and frequency f_i. The signals were formed from the data N_+ and N_- for $+\frac{1}{2}\pi$ and $-\frac{1}{2}\pi$ phase shifts: $S = (N_+ - N_-)/(N_+ + N_-)$. $N_\pm$ contain only decays occurring after the second rf pulse. For the backward (forward) positrons, $S = +(-)S_0 \sin\Delta \times (T+\tau)$.

For each run, we reduce p_i, t_i to the equivalent pressure P_i of an ideal gas at 0 °C. Slight variations of density (<4%) from run to run are compensated by renormalizing f_i to its equivalent F_i at the mean pressure $\langle P\rangle$ using the atomic fractional pressure shift for each gas. We then fit the relation $S_i = S_0 \sin(F_0 - F_i)2\pi(T+\tau)$ for the parameters S_0, F_0, treating forward and backward decays separately.

There are two ways to obtain N_+ and N_-. First, we can scale the superpositrons occurring after $T+2\tau = 3.7$ μsec; in this case $N\pm$ represents the content of the appropriate scaler. Second, we can use the time distributions from the digitron, which give $N_\pm(t)$ in 0.1-μsec bins. The contents of the channels from $t = T+2\tau$ to $t = 10$ μsec are then added to obtain $N_\pm$. Tables II and III present the results of the analysis of both scaler and digitron signals. All signals are corrected for $t<0$ background (accidentals). The results for scaler and digitron data are seen to be consistent. Figure 16 shows a typical resonance, with the least-squares fit for $S = S_0 \sin\Delta(T+\tau)$. The signal in the figure is the sum of forward and (−) backward signals.

We are interested in the possibility of "aging" effects on the resonant signal.[1,2,4] If any depolarization mechanisms were present, one would expect a decreasing signal at late decay times. Since the present experiment has the peculiar feature of yielding a constant signal after $T+2\tau$, it provides the opportunity for a sensitive test for any such depolarization.

We tested for time dependence in two ways. First, we examined the time dependent signal after a single rf pulse (see Fig. 17). No decrease in signal height is observed. Second, in our analysis of the digitron data, we fitted for $S(\Delta)$ in each of three time bins following the second rf pulse. No effect was resolved, as indicated by the results shown in Tables II and III.

VIII. RESULTS AND CONCLUSIONS

The final values of $\Delta\nu(P)$ from the scaler data of Table II are

$$\Delta\nu(6469\ \text{Torr, Kr}) = 4462\,999.78(2.96)\ \text{kHz} \times (0.65\ \text{ppm}), \qquad (57)$$

TABLE II. Results of fits to $S = S_0 \sin(\nu - \nu_0)2\pi(T+\tau)$: forward decays $\nu_0 = 4463$ MHz $+ f_0$(kHz).

Gas		Scaler data	Bin 1 $\tau = 4.2$–4.9 μsec	Bin 2 $\tau = 5.0$–6.6 μsec	Bin 3 $\tau = 6.7$–8.7 μsec	Bins 1–3 Composite
2742 Torr Kr	f_0	170.56(2.76)	163.13(4.14)	172.09(3.78)	166.51(5.79)	169.54(2.52)
	S_0	1.29(14)	1.30(20)	1.24(17)	1.05(22)	1.21(11)
	χ^2/N	50/62	50/62	60/62	66/62	59/62
6469 Torr Kr	f_0	007.30(4.92)	001.72(8.73)	008.74(5.70)	001.54(7.17)	005.05(3.96)
	S_0	1.47(22)	1.24(35)	1.67(30)	1.65(39)	1.54(20)
	χ^2/N	26/19	26/19	24/19	8/19	19/19
7150 Torr Ar	f_0	158.65(4.11)	162.04(5.94)	163.33(6.57)	151.43(9.03)	160.27(3.96)
	S_0	1.68(24)	1.88(38)	1.48(32)	1.32(44)	1.56(21)
	χ^2/N	10/20	15/20	8/20	16/20	13/20

$$\Delta\nu(2742\ \text{Torr, Kr}) = 4463\,173.26(1.90)\ \text{kHz} \times (0.45\ \text{ppm}), \quad (58)$$

$$\Delta\nu(7150\ \text{Torr, Ar}) = 4463\,152.17(2.37)\ \text{kHz} \times (0.5\ \text{ppm}). \quad (59)$$

The quoted errors are standard deviations based on statistics alone. We could not identify any effects which would shift the frequency at which the signal crosses zero by an amount significant at this level. Among the effects considered were (a) unequal amplitudes or widths of the two rf pulses; (b) departure of $|\varphi|$ from $\frac{1}{2}\pi$, (c) difference between the cavity and the oscillator frequencies; (d) effects of static fields; and (e) time structure of the rf pulses.

While the vacuum value $\Delta\nu(0)$ is of direct interest in determining α, experiments always actually measure $\Delta\nu(p)$, i.e., the hfs splitting of muonium in a buffer gas at some finite pressure p. These quantities can be related by

$$\Delta\nu(p) = \Delta\nu(0)[1 + ap + bp^2 + \cdots], \quad (60)$$

where a is the customary fractional pressure-shift coefficient (FPS), already well known for many atoms in various host gases from optical pumping studies. In these studies the pressure is generally so low (<100 Torr) that the quadratic term b can well be neglected, and $\Delta\nu(0)$ obtained by linear extrapolation to zero density.

Extrapolating Eqs. (57) and (58) linearly, we obtain

$$\Delta\nu(0\ \text{Torr, Kr}) = 4463\,301.3(4.1)\ \text{kHz}\ (0.88\ \text{ppm}) \quad (61)$$

and a coefficient of fractional (linear) pressure shift (FPS)

$$a(\text{Kr}) = -10.47(21)\times10^{-9}\ \text{Torr}^{-1}. \quad (62)$$

Both $\Delta\nu$ and a are in excellent agreement with earlier, less accurate results from this laboratory[2] and from Yale.[4] a agrees furthermore with the value $-10.4(2)\times10^{-9}$ Torr^{-1} reported[25] for atomic H in Kr. It hence appears appropriate to extrapolate Eqs. (57) and (58) together with the data from Ref. 2; this yields

$$\Delta\nu(0\ \text{Torr, Kr}) = 4463\,301.2(2.3)\ \text{kHz}\ (0.5\ \text{ppm}), \quad (63)$$

$$a(\text{Kr}) = -10.37(7)\times10^{-9}\ \text{Torr}^{-1}. \quad (64)$$

Assuming that a(Ar) also has the same value for muonium as for H in Ar, $-4.78(3)\times10^{-9}$,[26] we extrapolate Eq. (59) linearly, obtaining

$$\Delta\nu(0\ \text{Torr, Ar}) = 4463\,304.71(2.56)\ \text{kHz}\ (0.6\ \text{ppm}) \quad (65)$$

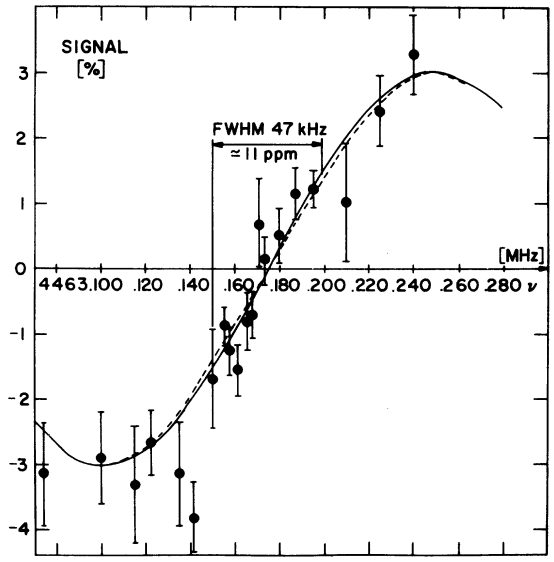

FIG. 16. Split-field resonance in 2740 Torr Kr. The solid curve is the least-squares fit to $S(\Delta) = S_0 \sin\Delta(T + \tau)$, with $\chi^2/N = 1.12$. The dashed curve is the computed signal, taking into account all effects discussed in Secs. II E and IV.

TABLE III. Results of fits to $S = S_0 \sin(\nu - \nu_0)2\pi(T + \tau)$: Backward decays $\nu_0 = 4463$ MHz $+ f_0$(kHz).

Gas		Scaler data	Bin 1 $\tau = 4.2 - 4.9\ \mu$sec	Bin 2 $\tau - 5.0 - 6.6\ \mu$sec	Bin 3 $\tau = 6.7 - 8.7\ \mu$sec	Bins 1 – 3 Composite
2742 Torr Kr	f_0	175.60(2.61)	181.96(3.57)	174.73(2.97)	181.57(6.00)	178.18(2.13)
	S_0	1.62(16)	1.79(22)	1.86(21)	1.21(25)	1.66(13)
	χ^2/N	60/62	63/62	78/62	55/62	65/62
6469 Torr Kr	f_0	−004.43(3.69)	011.65(5.82)	−005.87(4.20)	004.33(10.86)	001.78(3.06)
	S_0	2.84(34)	2.78(50)	3.30(45)	1.65(57)	2.78(30)
	χ^2/N	11/19	25/19	15/19	10/19	17/19
7150 Torr Ar	f_0	148.93(2.91)	158.86(7.20)	146.17(4.53)	152.80(5.64)	149.77(3.18)
	S_0	3.61(39)	2.36(60)	3.25(55)	3.30(68)	2.97(36)
	χ^2/N	13/20	18/20	14/20	12/20	14/20

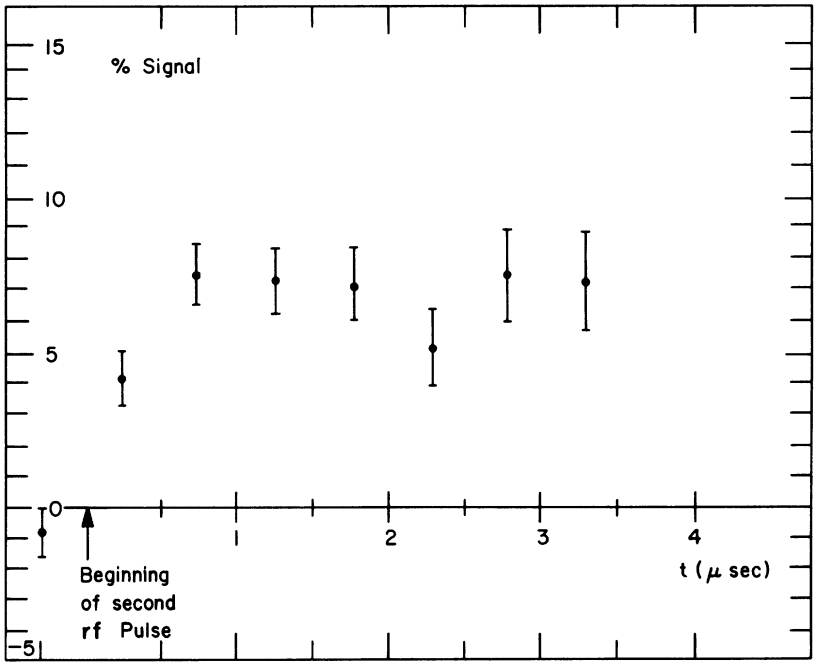

FIG. 17. Time-dependent signal for single-pulse data. There is no evidence for depolarization at late times.

in accord with both Eq. (63) and earlier work.[1,2,4]

Figure 18 is a plot of all available data on $\Delta\nu$ in Ar and Kr,[1,2,27] including Eqs. (57)–(59). Since all results are seen to be consistent, it is legitimate to fit them jointly to Eq. (60) to obtain a and b for each gas. The resulting fits are graphed together with fits to the linear term only. The results for $\Delta\nu(0)$, a, b are given in Table IV. We also fit the Ar and Kr data jointly, requiring the intercept $\Delta\nu(0)$ to be the same for both gases, and obtain

$$\Delta\nu(0) = 4463\,304.4(2.3)\ \text{kHz}\ (0.5\ \text{ppm}). \qquad (66)$$

This "world average" is in substantial agreement with Eqs. (63) and (65) and has the same accuracy.

In Eq. (63) we extrapolated our low-pressure Kr data linearly, anticipating the contribution of the quadratic term to be less than the experimental error. Using the fitted value of b(Kr) obtained above, the extrapolated $\Delta\nu(0)$ is shifted by 2.8 kHz, and indeed verifies the assumption.

To extract α from $\Delta\nu(0)$ of Eq. (66), we need a value for the muon magnetic moment. Adopting $\mu_\mu/\mu_p = 3.183\,347(9)$ as reported by Hague *et al.*,[13] Eq. (6) yields

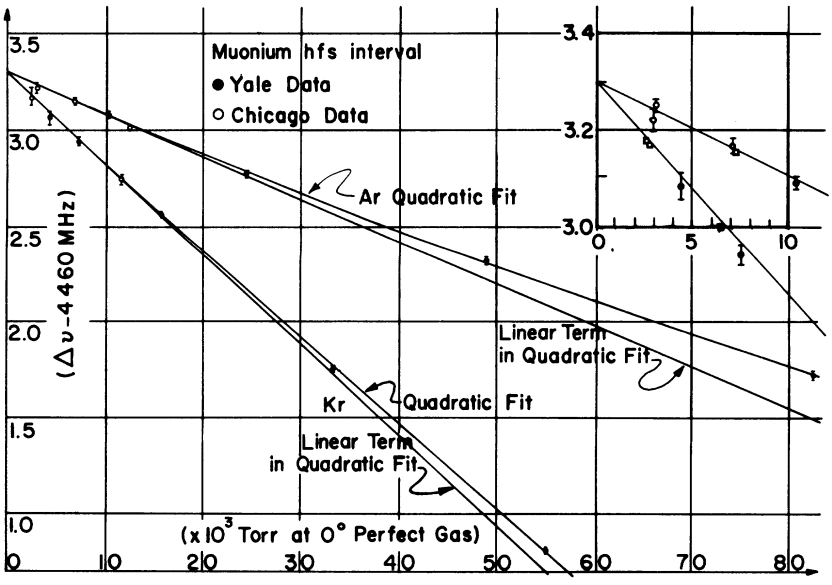

FIG. 18. Extrapolation of $\Delta\nu(P)$ to zero pressure. The curves show the least-squares fit to Eq. (60) for Ar and Kr, using all available data (Chicago and Yale). The linear term only in the quadratic fit is shown for comparison.

TABLE IV. Parameters obtained from a fit to $\Delta\nu(P)=\Delta\nu(0)\,[1+aP+bP^2]$.

Gas	$\Delta\nu(0)$ (kHz)	a (10^{-9} Torr^{-1})	b (10^{-15} Torr^{-2})	Input used
Ar	4463307.5(5.7)	−4.94(17)	7.8(2.1)	all Ar data
Kr	4463302.8(2.5)	−10.56(9)	7.8(1.8)	all Kr data
Ar *and* Kr	4463304.4(2.3)	Ar: −4.89(9)	Ar: 6.9(1.2)	joint fit to Ar
		Kr: −10.61(8)	Kr: 8.6(1.7)	and Kr constraining $\Delta\nu(0)$ to give the same value

$$\alpha^{-1}-137=0.036\,26(20)\ (1.5\ \text{ppm}), \tag{67}$$

whereas our result[2,28] $\mu_\mu/\mu_p=3.183\,349(15)$ yields

$$\alpha^{-1}-137=0.036\,31(32)\ (2.4\ \text{ppm}). \tag{68}$$

Equation (68) contains corrections for the g_j shift reported in Ref. 28. The current value of $(\alpha^{-1}-137)$ without QED is 0.036 08(26), in agreement with Eqs. (67) and (68).

The ratio of Eq. (2) with the corresponding formula for the hydrogen hyperfine interval[29] is

$$\frac{\Delta\nu(\mu e)}{\Delta\nu(pe)}=\frac{\mu_\mu}{\mu_p}\left(\frac{1+m_e/m_p}{1+m_e/m_\mu}\right)^3(1+\delta_\mu-\delta_p-\delta_p'). \tag{69}$$

Here $\delta_\mu=\delta_{\mu1}+\delta_{\mu2}=-174.1$ ppm, and $\delta_p=-33.5(9)$ ppm[30] are the relativistic recoil and finite size corrections, and δ_p' is the proton polarizability; various other electrodynamic corrections, identical for the two atoms, cancel in the ratio to first order. With Eq. (66) and $\Delta\nu(pe)=1420\,405.75$ kHz,[31] Eq. (69) yields either μ_μ/μ_p or δ_p':

$$\mu_\mu/\mu_p=3.183\,3318(33),\ \text{with}\ \delta_p'=0 \tag{70}$$

$$\delta_p'=5.4(4.8)\ \text{ppm},\ \text{with}\ \mu_\mu/\mu_p=3.183349(15). \tag{71}$$

This result for δ_p' is consistent with that obtained by comparing theory and experiment for $\Delta\nu(pe)$,[30] $\delta_p'=1.2(3.2)$ ppm.

Figure 19 shows a plot of $\Delta\nu(\mu e)$ and μ_μ/μ_p, and the resulting value of $(\alpha^{-1}-137)$. The novel technique described here will allow one to push the accuracy on $\Delta\nu(0)$ much further yet. A corresponding improvement in the knowledge of the muon magnetic moment will, however, be needed to make the accuracy useful.[7]

ACKNOWLEDGMENTS

This work was again made possible through gifts and loans from many individuals and companies. We would in particular like to thank Dr. E. Ginzton (Varian) for a VSC9620C oscillator, E. Taylor (Litton) for an L-5116 traveling-wave tube, and P. Damrel (Texas Instruments) for parts of a precision gauge. We are indebted to H. Kautzky, M. Neumann, R. Norton, and T. A. Nunamaker for continued engineering support, and to R. Wall and J. Roehrig for technical assistance. Finally, we wish to thank A. Magnon for many contributions to the preparatory stages of this work.

APPENDIX A: STATISTICAL OPTIMIZATIONS

1. No Accidentals

a. Split-field resonance. The number of decays observed in the forward- and backward-decay positron telescopes after the second rf pulse ($t>T'=T+\tau$) is

$$N_{f(b)}(\Delta)=e^{-T'/\tau_\mu}\{N_{A1}+N_{gas}[1+(-)S_0 f(2b/a)^2\times\cos(\Delta T'+\varphi)]\}. \tag{A1}$$

N_{A1} is the number of decays correlated with muons not stopping in the gas but triggering a stop signature, and N_{gas} is number of decays correlated with muons stopping in the gas. The quantities N_{A1}, N_{gas},

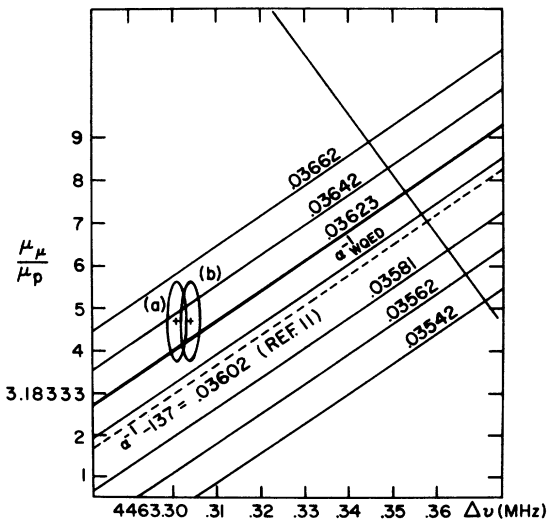

FIG. 19. $(\alpha^{-1}-137)$ vs μ_μ/μ_p and $\Delta\nu$. The values of $\Delta\nu$ from (a) Eq. (63) (*linear fit*) and (b) Eq. (66), together with μ_μ/μ_p of Ref. 13, yield values of $(\alpha^{-1}-137)$in good agreement with the recommended value (Ref. 11) (dashed line). Heavy lines indicate standard deviations in the latter value.

S_0 are different for forward and backward decays, and $S_{0f} < 0$ while $S_{0b} < 0$.

We form the signal from data N_+, N_- with $= \pm\frac{1}{2}\pi$:

$$S_{f(b)}(\Delta) = \frac{N_+ - N_-}{N_+ + N_-} = -(+) S_0 f (2b/a)^2 \sin\Delta(T+\tau). \quad \text{(A2)}$$

The total number of decays observed is $N_e = 2(N_{Al} + N_{gas})$. The error on the signal $S(\Delta)$ is

$$\sigma(S) = e^{\gamma T'/2}/\sqrt{N_e}.$$

For $b \gg \Delta$, $a \simeq 1$. We define the parameters β, ν, and the estimators S_0', Δ':

$$S_0 = S_0' + \beta, \quad \Delta = \Delta' + \nu.$$

We now linearize $S(\Delta)$ in the parameters β, ν and optimize the error in the zero crossing frequency:

$$S(\Delta) = (S_0' + \beta) f \sin(\Delta' + \nu) T',$$
$$\simeq f S_0' \sin\Delta' T' + f\beta \sin\Delta' T' + f S_0' \nu T' \cos\Delta' T'. \quad \text{(A3)}$$

We define an interval $-l < \Delta < l$ in frequency over which the data is uniformly distributed. The error $\sigma(\omega_0)$ on the zero crossing determination is

$$\sigma(\omega_0) = \frac{e^{T'/2\tau_\mu}}{f S_0 T' \sqrt{N_e}} \left(\frac{1}{2l} \int_{-l}^{l} \cos^2 \Delta T' d\Delta \right)^{-1/2}$$
$$= \frac{\sqrt{2}\, e^{T'/2\tau_\mu}}{f S_0 T' \sqrt{N_e}} \left(1 + \frac{\sin 2lT'}{2lT'} \right)^{-1/2}. \quad \text{(A4)}$$

$\sigma(\omega_0)$ is minimum for $l = 0$, corresponding to taking all the data at the zero crossing:

$$\sigma(\omega_0) = e^{T'/2\tau_\mu}/f S_0 T' \sqrt{N_e}. \quad \text{(A5)}$$

We also optimize the pulse separation T'. $\sigma(\omega_0)$ is minimum for $T' = 2\tau_\mu$:

$$\sigma_{SF}(\omega_0) = e/2 f S_0 \tau_\mu \sqrt{N_e}. \quad \text{(A6)}$$

Converting from angular frequency to Hz gives Eq. (29):

$$\sigma_{SF}(\Delta\nu) = 0.216/f S_0 \tau_\mu \sqrt{N_e}.$$

b. Conventional 2-level cw resonance. The number of decays in the backward and forward telescopes is

$$N_{f(b)}(\Delta) = N_{Al} + N_{gas}[1 \pm S_0 L(\Delta)],$$

where

$$L(\Delta) = (2b)^2/(a^2 + \gamma^2). \quad \text{(A7)}$$

We form the signal from data with rf on and rf off:

$$S(\Delta) = \frac{N_{on} - N_{off}}{N_{on} + N_{off}} = \tfrac{1}{2} f S_0 L(\Delta), \quad \sigma(S) = 1/\sqrt{N_e}. \quad \text{(A8)}$$

Again we linearize in β, ν:

$$S(\Delta) \simeq \tfrac{1}{2} f S_0' L(\Delta) + \tfrac{1}{2} f\beta L(\Delta) - f S_0' \Delta\nu L^2(\Delta)/(2b)^2. \quad \text{(A9)}$$

We optimize for a uniform distribution of data over the frequency interval $-l < \Delta < l$:

$$\sigma(\omega_0) = \frac{(2b)^2}{f S_0 \sqrt{N_e}} \left(\frac{1}{2l} \int_{-l}^{l} L^4(\Delta) \Delta^2 \, d\Delta \right)^{-1/2}. \quad \text{(A10)}$$

We calculated the above integral numerically[32] and maximized it to obtain $l \simeq [(2b)^2 + \gamma^2]^{1/2}$:

$$\sigma(\omega_0) \simeq \frac{7.5b}{f S_0 \sqrt{N_e}} \frac{[(2b)^2 + \gamma^2]^{3/2}}{(2b)^3}. \quad \text{(A11)}$$

$\sigma(\omega_0)$ is minimum for $b = \gamma/\sqrt{2}$. Thus, for optimum power and data-taking interval,

$$\sigma_L(\omega_0) \simeq 10/f S_0 \tau_\mu \sqrt{N_e}. \quad \text{(A12)}$$

Converting to frequency units, we have Eq. (25):

$$\sigma_L(\Delta\nu) = 1.56/f S_0 \tau_\mu \sqrt{N_e}.$$

2. Accidentals

a. Split-field resonance. In the split-field experiment, we wait a time T' after a muon stop ($t = 0$) before looking for decays; the rate of cor-

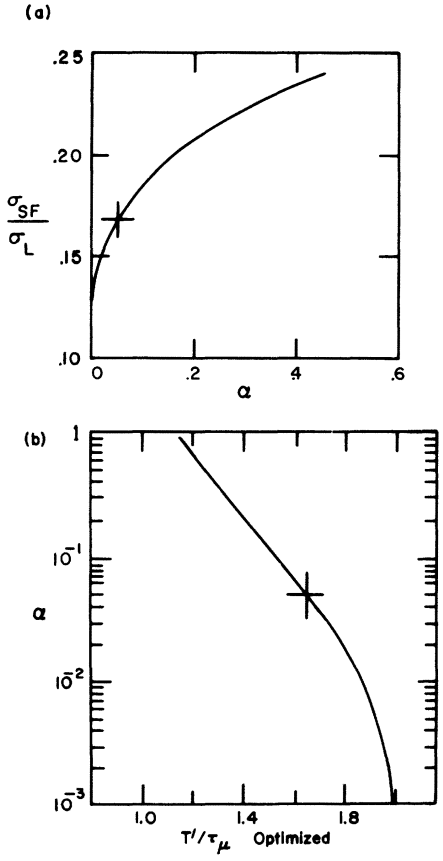

FIG. 20. Statistical optimization of data-taking parameters. (a) dependence of σ_{SF}/σ_L on the accidentals contamination α; (b) optimized pulse separation T'/τ_μ as a function of α.

related decays decreases exponentially during that time. The rate of accidental coincidences between a muon stop and an uncorrelated positron is time independent, and thus enhanced a factor $e^2 = 7.5$ relative to the correlated events.

We define N_a to be the number of accidental decays in the interval $0 < t < \tau_\mu$, for a sample of data with N_e time-correlated decays. If we accept all decays in the interval $T' < t < T_0$, we will see $N_a \gamma T_0$ accidentals and $N(\Delta)(1 - e^{-\gamma T_0})$ decays.

We define $R = e^{-\gamma T'}(1 - e^{-\gamma T_0})$. For the split-field resonance, the signal is

$$S_a(\Delta) = \frac{S_0 N_e R \sin \Delta T'}{N_e R + 2N_a \gamma T_0} \frac{N_e R S(\Delta)}{N_e R + 2N_a \gamma T_0},$$

$$\sigma(S_a) = [N_e R + 2N_a \gamma T_0]^{-1/2} = \sigma(S)\left(\frac{N_e e^{-\gamma T'}}{N_e R + 2N_a \gamma T_0}\right)^{1/2}. \tag{A13}$$

The resulting error on the zero-crossing frequency is

$$\sigma_a(\nu) = \sigma(\nu) \frac{\sigma(S_a)}{\sigma(S)} \frac{S(\Delta)}{S_a(\Delta)} = \left(\frac{N_e R + 2N_a \gamma T_0}{R f S_0 T' N_e}\right)^{1/2}. \tag{A14}$$

The ratio $\alpha = \gamma T_0 N_a / N_e$ is the fraction of accidentals in the decays during the interval $0 < t < T_0$. $\sigma_a(\nu)$ is minimum for

$$\gamma T' = 2\left(1 - \frac{2\alpha}{R} e^{-2\gamma T_0}\right)$$

or for

$$\alpha = \frac{2e^{-\gamma(T' + T_0)}}{1 - (2\gamma T_0/R)e^{-2\gamma T_0}}. \tag{A15}$$

Figure 20 shows a plot of $\sigma_a(\nu)$, optimized for $\gamma T'$, versus α. In our experiment, we used $T' = 3.4$ μsec for an accidentals contamination of $\alpha \simeq 5\%$.

b. Conventional 2-level CW resonance. The signal for CW resonance with accidentals is

$$S_a(\Delta) = \frac{N_e L(\Delta)(1 - e^{-\gamma T_0})}{N_e(1 - e^{-\gamma T_0}) + 2N_a \gamma T_0} = \frac{N_e R L(\Delta)}{N_e R + 2N_a \gamma T_0}, \tag{A16}$$

$$\sigma(S_a) = \sqrt{N_e}\,\sigma(S)/(N_e R + 2N_a \gamma T_0)^{1/2}. \tag{A17}$$

We then obtain for the zero-crossing error:

$$\sigma_a(\nu) = [(N_e R + 2N_a \gamma T_0)^{1/2}/\sqrt{N_e}]\,\sigma(\nu), \tag{A18}$$

where $\sigma_a(\nu)$ is minimum for

$$\alpha = e^{-\gamma T_0}/[1 - 2\gamma T/(1 - e^{-\gamma T_0})].$$

This allows us to optimize T_0 for a given α.

The ratio $\sigma_{SF}^a(\Delta\nu)/\sigma_L^a(\Delta\nu)$ is plotted as a function of α. At the accidentals level $\alpha = 0.05$ in our experiment, $\sigma_{SF}/\sigma_L = 0.17$.

---

*Present address: University of Louvain, Belgium.
†Paper submitted by P. M. McIntyre to the Department of Physics, University of Chicago, in partial fulfillment of the requirement for the Ph.D degree.
‡Present address: Computer Sciences Corp., Washington, D. C.
§National Science Foundation trainee, 1969–1971.

[1]R. D. Ehrlich, H. Hofer, A. Magnon, D. Y. Stowell, R. A. Swanson, and V. L. Telegdi, Phys. Rev. A **5**, 2357 (1972).
[2]R. DeVoe, P. M. McIntyre, A. Magnon, D. Y. Stowell, R. A. Swanson, and V. L. Telegdi, Phys. Rev. Lett. **25**, 1779 (1970). The value of μ_μ/μ_p has been corrected for g_j pressure shifts (see Ref. 28); the corrected value is used in the present work.
[3](a) P. A. Thompson, J. J. Amato, P. Crane, V. W. Hughes, R. M. Mobley, G. zu Putlitz, and J. E. Rothenberg, Phys. Rev. Lett. 22, 163 (1968). (b) P. A. Thompson, thesis (Yale University, 1967) (unpublished).
[4]T. Crane, D. Casperson, P. Crane, P. Egan, V. W. Hughes, R. Stambaugh, P. A. Thompson, and G. zu Putlitz, Phys. Rev. Lett. **27**, 474 (1971).
[5]N. F. Ramsey, Phys. Rev. **78**, 695 (1950).
[6]N. F. Ramsey, *Molecular Beams* (Clarendon, Oxford, England, 1956), p. 124ff.
[7]The split-field technique can also be used to observe the strong-field Zeeman transitions ν_1, ν_2, allowing simultaneous measurement of $\Delta\nu$ and g'_μ. We are currently planning such an experiment.
[8]D. Favart, P. M. McIntyre, D. Y. Stowell, V. L. Telegdi, R. DeVoe, and R. A. Swanson, Phys. Rev. Lett. **27**, 1336 (1971); Phys. Rev. Lett. **27**, 1340 (1971).
[9]V. W. Hughes, Annu. Rev. Nucl. Sci. **16**, 445 (1966).
[10]T. Fulton, D. A. Owen, and W. W. Repko, Phys. Rev. Lett. **26**, 61 (1971).
[11]W. H. Parker, B. N. Taylor, and D. N. Langenburg, Rev. Mod. Phys. **41**, 375 (1969).
[12]N. Barash-Schmidt, A. Barbaro-Galtieri, L. R. Price, A. H. Rosenfeld, P. Soding, C. G. Wohl, M. Roos, and G. Conforto, Rev. Mod. Phys. **41**, 109 (1969).
[13]J. F. Hague, J. E. Rothenberg, A. Schenck, R. W. Williams, K. K. Young, and K. M. Crowe, Phys. Rev. Lett. **25**, 628 (1970).
[14]F. Bloch and A. Siegert, Phys. Rev. **57**, 552 (1940).
[15]Here we follow closely the work of Ramsey (see Ref. 5).
[16]The calculation of $\langle S_1 \rangle$, $\langle S_1 \rangle$ include all the effects discussed in Sec. IV, and are done by computer. The numerical techiques are detailed by P. M. McIntyre, thesis (University of Chicago, 1973)(unpublished).
[17]J. C. Slater, *Microwave Electronics* (Van Nostrand, New York, 1950), p. 43ff.
[18]W. G. Wadey, Rev. Sci. Instrum. **27**, 910 (1956).
[19]W. E. Cleland, J. M. Bailey, M. Eckhause, V. W. Hughes, R. M. Mobley, R. Prepost, and J. E. Rothenberg, Phys. Rev. Lett. **13**, 202 (1964).
[20]V. L. Stout and M. D. Gibbons, J. Appl. Phys. **26**, 1488 (1955).
[21]R. A. Swanson, Rev. Sci. Instrum. **31**, 149 (1960).
[22]Litton Industries Publ. No. 506, San Carlos, Calif., 1968 (unpublished).
[23]A. O. Weissenberg, *Muons* (North-Holland, Amsterdam, 1967), pp 160–165.
[24]All gas densities are expressed in equivalent torr for a perfect gas at 0 °C, using the virial data of J. A. Beattie, J. S.

Brierley, and R. J. Bariault, J. Chem. Phys. **20**, 1615 (1952).
[25]E. S. Ensberg and C. L. Morgan, Phys. Lett. **28A**, 106 (1968).
[26]R. A. Brown and F. M. Pipkin, Phys. Rev. **174**, 48 (1968).
[27]P. A. Thompson, D. Casperson, P. Crane, T. Crane, P. Egan, V. W. Hughes, G. zu Putlitz, and R. Stambaugh, in Proceedings of the International Conference on Precision Measurement and Fundamental Constants, 1970, p. 339 (unpublished).
[28]J. Jarecki and R. M. Herman, Phys. Rev. Lett. **28**, 199 (1972).
[29]For the corrections δ_μ, δ_p, δ'_p we follow the notation of R. S. Cole and W. W. Repko, Phys. Rev. Lett. **29**, 1295 (1972).
[30]The value of δ_p contains the order $(m_e/m_p)\alpha^2\ln\alpha^{-1}$ correction reported in Ref. 29.
[31]S. B. Crampton, D. Kleppner, and N. F. Ramsey, Phys. Rev. Lett. **11**, 338 (1963).
[32]The integral in Eq. (A10) has a closed-form solution: $(1/2l)\int_{-1}^{1} L^4(\Delta)\,\Delta^2\,d\Delta = [16b^8/(\gamma^2+4b^2)^3]\{(\tan^{-1}x/x) + [(3x^4+8x^2-3)/3(1+x^2)^3]\}$, where $x = l(\gamma^2+4b^2)^{-1/2}$ The maximum occurs at $x = 0.94$, in agreement with the numerically integrated result.